Genomic and metabolomic characterization of Acinetobacter calcoaceticus (DT1) and Citrobacter braakii (S10) reveal functional traits for plant stress alleviation and sustainable agriculture

Imen Ghazala
University of Sfax
Naïma Sayahi
University of Sfax
Abdelmalek Alioua
Institut de Biologie Moléculaire des Plantes (IBMP), CNRS, Université de Strasbourg
Valérie Cognat
Institut de Biologie Moléculaire des Plantes (IBMP), CNRS, Université de Strasbourg
Dimitri Heintz
Université de Strasbourg, CNRS, IPHC UMR7178
Claire Villette
Université de Strasbourg, CNRS, IPHC UMR7178
Julie Zumsteg
Institut de Biologie Moléculaire des Plantes (IBMP), CNRS, Université de Strasbourg
Moez Hanin
University of Sfax
Alexandre Berr
Institut de Biologie Moléculaire des Plantes (IBMP), CNRS, Université de Strasbourg
Chantal Ebel
chantal.ebel@isbs.usf.tn

University of Sfax

Research Article

Keywords: Plant growth-promoting rhizobacteria (PGPR), Acinetobacter calcoaceticus, Citrobacter braakii, Whole-genome sequencing, Metabolomic profiling

Posted Date: November 17th, 2025

DOI: https://doi.org/10.21203/rs.3.rs-7900185/v1

Additional Declarations: No competing interests reported.

Abstract

Plant growth-promoting rhizobacteria (PGPR) enhance plant growth and development through diverse mechanisms, including phytohormone production, nutrient acquisition, and stress mitigation. This study describes the isolation and characterization of two bacterial strains, DT1 and S10, from the rhizospheres of *Diplotaxis tenuifolia* and *Cynodon dactylon*, respectively capable of solubilizing phosphate and zinc, fix nitrogen and produce indole acetic acid (IAA) and siderophores. Using whole genome sequencing and taxonomic analyses, these two strains were identified as *Acinetobacter calcoaceticus* (DT1) and *Citrobacter braakii* (S10). Functional genomic annotation revealed numerous genes associated with key plant growth-promoting traits, including those involved in indole-3-acetic acid (IAA) (*trpABCDE*, *ipdC*), cytokinin (*miaABE*), and riboflavin biosynthesis, confirmed by targeted metabolomics. In addition, genes associated with nitrogen metabolism (*nirB*, *narGHI*) and phosphate solubilization (*gcd*, *phoARP*, *pstABCS*, *pqqEFG*) were identified and supported by phenotypic assays. Interestingly, biosynthetic gene clusters for the secondary metabolites enterobactin, bacillibactin, and staphyloferrin B, known to contribute to plant growth promotion, were identified in both genomes. Both strains also harbored genes encoding ACC deaminase, an enzyme known to enhance plant tolerance to abiotic stress. Furthermore, non-targeted metabolomic analysis revealed that DT1 and S10 produced a range of intracellular and extracellular metabolites associated with plant growth promotion and stress resilience, including cadaverine, biotin, arginine, and GABA. Collectively, these findings position DT1 and S10 as promising bioinoculant candidates, offering an integrative genomic and metabolic foundation for their application in next-generation sustainable agricultural strategies.

Introduction

Plant growth-promoting rhizobacteria (PGPR) represent a functionally diverse group of beneficial root-associated bacteria that colonize the rhizosphere and stimulate plant growth and development through a variety of direct and indirect mechanisms (Mmotla et al. 2025). Since their introduction by Kloepper and Schroth in the late 1970s, PGPR have been extensively studied for their potential to enhance agricultural productivity while promoting environmentally sustainable and low-input farming practices. PGPR act via both direct and indirect mechanisms. Direct effects include atmospheric nitrogen fixation (Masood et al. 2020) and solubilization of soil inorganic phosphorus, both of which enhance nutrient availability, as well as the production of phytohormones such as indole-3-acetic acid (IAA), cytokinins, and gibberellins, which collectively promote plant growth and development (Joshi et al. 2023). Indirect effects include pathogen suppression through siderophores production (Gao et al. 2022), activation of 1-aminocyclopropane-1-carboxylate (ACC) deaminase activity (Zafar-ul-Hye et al. 2019), emission of volatile organic compounds (VOCs) (Mhlongo et al. 2022) and synthesis of antimicrobial metabolites, leading to induced systemic resistance (ISR) (Li et al. 2024).

Various bacterial genera exhibit plant growth-promoting (PGP) potential, including *Pseudomonas* (Comeau et al. 2021), *Bacillus* (Husna et al. 2023), *Azospirillum* (Sun et al. 2025), *Citrobacter* (Ajmal et al. 2022), and *Acinetobacter* (Josephine and Thomas 2021). *Acinetobacter* spp. are Gram-negative,

oxidase-negative, aerobic bacteria that are non-motile due to the absence of flagella (Josephine and Thomas 2021). This genus is widely spread in nature and is frequently found in the rhizosphere of several plant species (Mujumdar et al. 2023). Previous research have demonstrated that certain *Acinetobacter* strains, including *A. calcoaceticus*, (Eswaran et al. 2024; Okla et al. 2025) possess PGP traits, including IAA production (Lin et al. 2018), inorganic phosphate solubilization (He and Wan 2021) and nitrogen fixation (Wu et al. 2022). Likewise, *Citrobacter* spp. are Gram-negative, facultatively anaerobic, oxidase-negative bacteria that are generally motile (Fanning et al. 2016). This genus has also been reported in several studies for its PGP potential (Ajmal et al. 2022; Fadiji et al. 2023).

In recent years, advances in high-throughput genomics and metabolomics have significantly deepened our understanding of PGPR diversity, functionality and their complex interactions with host plants (for review see Paterson et al., 2017). Furthermore, whole-genome sequencing (WGS) facilitates the identification of key genetic determinants responsible for plant-beneficial traits, including genes involved in nitrogen fixation (*nir*, *nar*), phosphate solubilization (*gcd*, *pqq*), auxin biosynthesis (*ipdC*), and secondary metabolite production (*ent*) (Thamvithayakorn et al. 2025; Zhang et al. 2024a; Li et al. 2024). In parallel, metabolomic profiles enable the identification of bioactive compounds produced by PGPR, including signaling molecules, growth regulators, and stress-related metabolites, thereby bridging genotypic potential with phenotypic expression (Mashabela et al. 2023).

In this study we isolated two bacterial strains S10 and DT1 from the rhizospheres of *Cynodon dactylon* and *Diplotaxis tenuifolia*, respectively. These strains exhibited multiple PGP traits and were taxonomically classified, based on WGS analyses, as *Acinetobacter calcoaceticus* (DT1) and *Citrobacter braakii* (S10). Functional genome annotation unveiled numerous genes associated with plant growth promotion, while targeted and non-targeted metabolomic profiling revealed a variety of metabolites implicated in growth stimulation and abiotic stress tolerance.

Materials and methods

Bacteria isolation

Rhizospheres samples of *Cynodon dactylon* and *Diplotaxis tenuifolia* were collected from wild areas in the Sfax region, located in central Eastern coast of Tunisia (34°39'N, 10°43'E). One gram of rhizospheric soil from each plant was suspended in 10 mL of sterile water and serially diluted. Subsequently, 100 µL from the 10^{-6} and 10^{-7} dilutions of each suspension were plated onto a culture medium composed of: K_2HPO_4 (0.3 g/L), KH_2PO_4 (0.3 g/L), KCl (0.1 g/L), NaCl (1 g/L), $CaCl_2$ (0.1 g/L), yeast extract (1 g/L), peptone (5 g/L), glucose ($C_6H_{12}O_6$, 5 g/L), and agar (18 g/L) (Sayahi et al. 2022). After 48 hours of incubation at 30°C, isolated colonies were selected and subcultured onto fresh plates to ensure purity. The purified isolates (named hereafter S10 and DT1) were cultivated on Luria-Bertani (LB) medium at 37°C, maintained at 4°C prior to use, and preserved as glycerol stocks at − 80°C.

Plant Growth-Promoting (PGP) traits

Siderophore production

Siderophore production by S10 and DT1 isolates was evaluated using the Chrome Azurol S (CAS) agar method, as described by Schwyn and Neilands (1987), with slight modifications. Briefly, the CAS reagent was prepared by mixing 60.5 mg of Chrome Azurol S with an iron (III) solution (1 mM $FeCl_3$ in 10 mM HCl) and 72.9 mg of hexadecyltrimethylammonium bromide (HDTMA) to form a blue-colored complex. This solution was then added to a low-iron minimal medium at 10% (v/v) before pouring into Petri dishes. Bacterial isolates were streaked onto the CAS agar and incubated at 30°C for 24–48 hours. The appearance of an orange or yellow halo around the streak line indicated siderophore production.

Phosphate and zinc solubilization

The ability of S10 and DT1 isolates to solubilize insoluble phosphate and zinc compounds was evaluated using agar plate assays. For phosphate solubilization, isolates were spot-inoculated onto Pikovskaya's agar medium containing tricalcium phosphate ($Ca_3(PO_4)_2$) as the sole phosphorus source (Pikovskaya 1948). For zinc solubilization, isolates were grown on Yeast Extract Dextrose (YED) medium supplemented with zinc oxide (ZnO) as the insoluble zinc sources (Saravanan et al. 2007). In both assays, plates were incubated at 30°C for 2 to 5 days. Solubilization was evidenced by the formation of clear halos around the bacterial colonies. All experiments were conducted in triplicate to ensure consistency and reproducibility.

Indole-3-acetic acid (IAA)

The production of indole-3-acetic acid (IAA) by S10 and DT1 isolates was investigated using Salkowski reagent. Each isolate was inoculated into 25 mL of LB medium supplemented with 5 mM of L-tryptophan and incubated at 30°C for 24 to 48 hours under shaking conditions (150 rpm). After incubation, cultures were centrifuged at 10,000 rpm for 10 minutes, and 1 mL of the cell-free supernatant was mixed with 2 mL of Salkowski reagent (2% 0.5M $FeCl_3$ in 35% perchloric acid). The mixture was incubated in the dark at room temperature for 30 minutes. A pink coloration indicated the presence of IAA, and absorbance was then measured at 530 nm using a spectrophotometer (Sobarzo et al. 2013). IAA concentration was determined by comparison with a standard curve of pure IAA. All experiments were performed in triplicate.

Nitrogen fixation

The nitrogen-fixing ability of S10 and DT1 was tested using the Nitrogen-Free Broth (NFB) medium as described by Siddikee et al. (2010). In brief, isolates were inoculated onto NFB plates and incubated at

30°C for 2 to 5 days. Bacterial growth on nitrogen-free medium was considered indicative of nitrogen fixation capacity. All experiments were conducted in triplicate.

DNA extraction, genome sequencing and assembly

Genomic DNA was extracted from overnight bacterial cultures using the Qiagen Genomic-tip 100/G kit (Qiagen, Cat. No. 10243). Approximately 10–20 µg of high molecular weight DNA was obtained per extraction, with concentrations measured using the Qubit™ dsDNA HS Assay Kit (Thermo Fisher Scientific). DNA purity was assessed by spectrophotometry, aiming for A260/280 ratios of ~ 1.8 and A260/230 ratios above 2.0. Oxford Nanopore libraries were prepared using the Native Barcoding Kit 24 V14 (SQK-NBD114.24, Oxford Nanopore Technologies) following the manufacturer's protocol, using ~ 1 µg of input DNA. Sequencing was performed on R10.4.1 PromethION flow cells (FLO-PRO114M) with MinKNOW software version 22.07.9.

The raw fast5 data generated by the MinKNOW software were basecalled and demultiplexed using Guppy v6.5.7 (Wick et al. 2019) with the super accuracy model dna_r10.4.1_e8.2_400bps_hac_prom and a minimum Q-score threshold of 7 to obtain the fastq files. Read quality was assessed with NanoPlot v0.32.1 (De Coster and Rademakers 2023), and the adapter sequences were trimmed with Porechop v0.2.4 (https://github.com/rrwick/Porechop). To evaluate potential contamination and obtain a preliminary taxonomic classification, reads were screened against the standard Kraken database using Kraken2 v2.0.9-beta (Wood et al. 2019). Genome assembly was performed with NextDenovo v2.5.2 (Hu et al. 2024) using default parameters, followed by polishing with NextPolish v1.4.1 (Hu et al. 2020) to correct base-level errors. Assemby quality and completeness were evaluated using QUAST v5.0.2 (Gurevich et al. 2013), including the BUSCO option to detect conserved orthologs and CheckM v1.2.2 (Parks et al. 2015). Final assemblies were reoriented at the *dnaA* gene using the Circlator fixstart tool v1.5.5 (Hunt et al. 2015).

Genome annotation

Genomic relatedness between strains was estimated based on the Average Nucleotide Identity (ANI) and digital DNA–DNA hybridization (dDDH). ANI values were calculated using the JSpecies Web Server (JSpeciesWS) (Richter et al. 2015), while dDDH values were obtained using the Type (Strain) Genome Server (TYGS) (Meier-Kolthoff and Göker 2019). Additionally, TYGS was used to construct a whole-genome phylogenetic tree based on the Genome Blast Distance Phylogeny (GBDP) approach.

The annotated genomes were uploaded to the MicroScope platform (https://mage.genoscope.cns.fr/microscope/home/index.php) and analyzed using the integrated genome annotation tools available on the platform (Vallenet et al. 2020). Complementary annotation was performed using multiple pipelines such as RAST (Rapid Annotation using Subsystem Technology (Aziz et al. 2008), PROKKA (Galaxy Version 1.14.6) (Seemann 2014) implemented with default

parameters via Galaxy, and KEGG (Kyoto Encyclopaedia of Genes and Genomes) Automatic Annotation Server v2.1 (Moriya et al. 2007) to study metabolic pathways within the assembled genome. Both genome sequences have been submitted to NCBI database under the submission references SUB15592691 (Genome assembly of *Citrobacter braakii* S10) and SUB15592887 (Genome assembly of *Acinetobacter calcoaceticus* DT1).

Metabolomics analysis

Chemicals

Deionized water was filtered through a Direct-Q UV station (Millipore), isopropanol and methanol were purchased from Fisher Chemicals (Optima ® LC/MS grade). NaOH was obtained from Agilent Technologies, acetic acid formic acid from Sigma Aldrich. Deuterated abscissic acid ($^2H_6$ ABA) obtained from OlChemIm was used as an internal standard. Standards were used to develop the UHPLC-TQ-MS/MS methods: abscisic acid (ABA), 6-benzylaminopurine (BAP), indole-3-butyric acid potassium salt (IBA), salicylic acid (SA), trans zeatin (t-zea) and tryptophan were purchased from Sigma; benzoic acid (BA), and gibberellic acid (GA3) were purchased from Fluka; brassinolide (BR), cis-12-oxo-phytodienoic acid (OPDA), castasterone (CS), cathasterone (CT), dinor-12-oxo-phytodienoic acid (dnOPDA), gibberellins A1, A4, A7 and GA20 (GA1, GA4, GA7, GA20), jasmonic acid (JA), jasmonic acid-isoleucine (JA-lLE), jasmonic acid-phenylalanine (JA-Phe), jasmonic acid-valine (JA-Val), 12-hydroxy-jasmonic acid (12-0H JA), and orobanchol (Oro) were purchased from OlChemim; indole-3-acetic acid (lAA) was purchased from Serva, and 6-furfurylaminopurine (kinetin, KIN), 6-(y, y-dimethylallylamino) purine (2iP) were purchased from Duchefa. 12-hydroxy-jasmonic acid-isoleucine (12-0H-JA-Ile), 12-carboxy-jasmonic acid (12-COOH-JA) and 12-carboxy jasmonic acid-isoleucine (12-COOH-JA-Ile) were generous gifts from Dr. Patrick Wehrung.

Sample preparation

A culture of S10 and DT1 was prepared by inoculating 10^7 spores/mL in a 50 mL falcon containing 10 mL of LB medium. Cultures were grown 24 hours at 28°C under continuous shaking at 180 rpm and cells were pelleted (5500 rpm, 10min). Pellets (40–60 mg fresh weight) were extracted with 5 volumes of cold methanol spiked with $^2H_6$ ABA (1µg/mL) and centrifuged (13,200 rpm; 10 min, 4°C) to recover the liquid phase for further analysis. The supernatant was prepared through solid phase extraction (5 mg, Oasis HLB, Waters) microplates. The phase was washed with 1 mL 80% MeOH and 1 mL 100% H_2O, then 500 µL of acidified supernatant (0.1% formic acid) was applied. A wash was performed with 1mL 2% MeOH, 0.1% formic acid before elution of the samples with 250 µL of 80% MeOH, 0.1% formic acid.

Non-Targeted Metabolomic Analysis

Samples were analyzed using liquid chromatography coupled to high resolution mass spectrometry on an UltiMate 3000 system (Thermo) coupled to an Impact II (Bruker) quadrupole time-of-flight (Q-TOF) spectrometer. Chromatographic separation was performed on an Acquity UPLC ® HSS T3 C18 column

(2.1x100 mm, 1.8 µm, Waters) equipped with and Acquity UPLC ® HSS T3 C18 pre-column (2.1x5 mm, 1.8 µm, Waters) using a gradient of solvents A (Water, 0.1% formic acid) and B (MeOH, 0.1% formic acid). Chromatography was carried out at 35°C with a flux of 0.3 $mL.min^{-1}$, starting with 2% B for 2 min, reaching 100% B at 10 min, holding 100% for 3 min and coming back to the initial condition of 5% B in 2 min, for a total run time of 15 min. Samples were kept at 4°C, 10 µL were injected in full loop mode with a washing step after sample injection with 150 µL of wash solution (H_2O/MeOH, 90/10, v/v). The spectrometer was equipped with an electrospray ionization (ESI) source and operated in positive ion mode on a mass range from 100 to 1000 Da with a spectra rate of 8 Hz in AutoMS/MS fragmentation mode. The end plate offset was set at 500 V, capillary voltage at 2500 V, nebulizer at 2 Bar, dry gas at 8 $L.min^{-1}$ and dry temperature at 200°C. The transfer time was set at 20–70 µs and MS/MS collision energy at 80–120% with a timing of 50–50% for both parameters. The MS/MS cycle time was set to 3 seconds, absolute threshold to 816 cts and active exclusion was used with an exclusion threshold at 3 spectra, release after 1 min and precursor ion was reconsidered if the ratio current intensity/previous intensity was higher than 5. A calibration segment was included at the beginning of the runs allowing the injection of a calibration solution from 0.05 to 0.25 min. The calibration solution used was a fresh mix of 50 mL isopropanol/water (50/50, v/v), 500 µL NaOH 1M, 75 µL acetic acid and 25 µL formic acid. The spectrometer was calibrated on the $[M + H]^+$ form of reference ions (57 masses from m/z 22.9892 to m/z 990.9196) in high precision calibration (HPC) mode with a standard deviation below 1 ppm before the injections for each polarity mode, and re-calibration of each raw data was performed after injection using the calibration segment.

Raw data were processed in MetaboScape 4.0 software (Bruker): molecular features were considered and grouped into buckets containing one or several adducts and isotopes from the detected ions with their retention time and MS/MS information when available. The parameters used for bucketing are a minimum intensity threshold of 10000, a minimum peak length of 3 spectra, a signal-to-noise ratio (S/N) of 3 and a correlation coefficient threshold set at 0.8. The $[M + H]^+$, $[M + Na]^+$, $[M + K]^+$, $[M + NH4]^+$ and $[M-H_2O + H]^+$ ions were considered. The obtained list of buckets was annotated using NPA (https://www.npatlas.org/), KNApSAcK (http://www.knapsackfamily.com/), FooDB (http://foodb.ca), PlantCyc (https://plantcyc.org/), PhenolExplorer (http://phenol-explorer.eu/), ECMDB (https://ecmdb.ca/) and YMDB (https://www.ymdb.ca/) to achieve level 3 annotations on the Schymanski scale (DOI: 10.1021/es5002105) with a maximum mass deviation of 3ppm and a maximum mSigma value of 30 (assessing the good fit of the isotopic profile). Spectral libraries were used to achieve Schymanski level 2 annotations with a minimum score of 800.

Targeted Metabolomic Analysis

Samples were analyzed by ultrahigh-performance liquid chromatography (UHPLC) on the UltiMate 3000 UHPLC system (Thermo) coupled to an EvoQ Elite LC-TQMS/MS (Bruker) mass spectrometer equipped with an electrospray ionization (ESI) source in MS/MS mode.

The samples were kept at 4 °C before injection of 5 µL in full loop mode, and chromatographic separation on an Acquity UPLC ® HSS T3 C18 column (2.1 X 100 mm, 1.8 µm, Waters) coupled to an Acquity UPLC HSS T3 C18 precolumn (2.1 x 5 mm, 1.8 µm, Waters). Samples were carried through the column following a gradient of solvent A (H_20; 0.1% formic acid) and B (methanol; 0.1% formic acid) at a flux of 0.300 mL min^{-1} starting with 5% B for 2 min, reaching 100% B at 10 min, holding 100% B for 3 min and returning to 5% B in 2 min, for a total run time of 15 min. The column was operated at 35 °C. Nitrogen was generated from pressurized air by a Nitro 35 nitrogen generator (GenGaz) and used as cone gas (30 L h^{-1}), heated probe gas (30 L h^{-1}) and nebulizer gas (35 L h^{-1}). The cone and heated probe temperatures were 350 and 300°C, respectively, and the capillary voltage was set at 3.5 kV. Phytohormones and bioactive metabolites were analyzed by multiple reaction monitoring (MRM) after determining the retention time and mode (positive or negative) by scan and the cone voltage, daughter ion and collision energy using the MRM builder function on standards. Wash solvent (80% H_20, 20% MeOH) was used to wash the syringe. A mix of the different standards served as a positive control.

Results

Isolation and Evaluation of Plant Growth-Promoting Traits in Rhizospheric Bacterial Strains

To identify PGPB strains adapted to harsh environments, rhizosphere samples of *Cynodon dactylon* and *Diplotaxis tenuifolia* were collected from wild arid areas. Pure bacterial cultures were obtained from the rhizospheric soils of both plants using the serial dilution technique. Among the thirty distinct isolates recovered on nutrient agar (NA), two strains (S10 and DT1 from *Cynodon dactylon* and *Diplotaxis tenuifolia* rhizospheres, respectively), were selected based on their distinct morphological characteristics. On nutrient agar, S10 produced smooth, greyish colonies, whereas DT1 produced opaque colonies. These two strains were subsequently used to evaluate their plant growth-promoting (PGP) potential. As shown in Table 1, both S10 and DT1 were able to grow on nitrogen-free medium, indicating their nitrogen-fixing capacity. In phosphate solubilization assays, both strains produced clear halos on Pikovskaya’s inorganic phosphate medium, while only S10 was able to solubilize zinc (Table 1, Fig. S1). The appearance of yellow halo around streak lines S10 and DT1 on Chrome Azurol S (CAS) agar showed their ability to produce siderophores (Table 1, Fig. S1c). Additionally, IAA production by strains S10 and DT1, in the presence of tryptophan, was quantified using Salkowski's reagent, yielding concentrations of 4.25 and 14.65 µg/mL, respectively (Table 1). Together, these results indicate that the newly isolated rhizobacterial strains S10 and DT1 exhibit promising plant growth-promoting traits.

Table 1
Plant growth-promoting (PGP) traits of the selected bacterial isolates *Citrobacter braakii* S10 and *Acinetobacter calcoaceticus* DT1.

Plant growth-promoting trait	*Citrobacter braakii* S10	*Acinetobacter calcoaceticus* DT1
Phosphate solubilization	+	+
Zinc solubilization	+	-
Nitrogen fixation	+	+
Siderophore production	+	+
IAA production (µg/ml)	4.25	14.65

+, positive; -, negative result for the test

General Genomic Features of S10 and DT1

To gain insight into the genomic architecture of the two selected PGPR strains, S10 and DT1, Whole Genome Sequencing (WGS) was performed. The sequencing output revealed that both strains possess a single circular chromosome (Fig. S2) and a summary of their genomic features is presented in Table 2. The genome of strain S10 is notably larger than that of DT1, comprising a total size of 4,913,851 bp, compared to 3,930,652 bp for strain DT1. Consistently, the number of predicted protein-coding genes was also higher in S10 (4,774 genes) than in DT1 (3,818 genes). The G + C content differed substantially between the two strains, with S10 exhibiting a value of 52.04%, whereas DT1 displayed a markedly lower G + C content of 38.75%, indicating their distinct taxonomic origins. Non-coding RNA elements also highlighted the divergence between the two genomes. S10 harbored a higher number of tRNA genes (84 vs. 73) and rRNA genes (25 vs. 18) than DT1, while both genomes contained a single copy of the transfer-messenger RNA (tmRNA) gene. Additionally, the number of miscellaneous RNAs (misc-RNAs), potentially including regulatory small RNAs, was much higher in S10 (82) compared to DT1 (30), suggesting a more complex regulatory potential in this strain. Another notable difference between the two genomes lies in the number of predicted pseudogenes (66 pseudogenes in S10 vs. 5 in DT1). Together, these genomic features reflect the phylogenetic divergence between the two strains and provide a foundational framework for further functional annotation and comparative analysis of the PGP traits.

Table 2
Genomic features of *Citrobacter braakii* S10 and *Acinetobacter calcoaceticus* DT1

Genomic Features	*Citrobacter braakii* S10	*Acinetobacter calcoaceticus* DT1
Genome size (bp)	4,913,851	3,930,652
G + C content (%)	52.04	38.75
N50	4913851	3930652
Number of contigs	1	1
Gene number	4,774	3,818
tRNA	84	73
rRNA	25	18
tmRNA	1	1
Misc-RNA	82	30
Pseudogenes	66	5

Whole Genome-Based Phylogenomic Identification of S10 and DT1

To assess the taxonomic affiliation of strains S10 and DT1, whole-genome-based phylogenetic and comparative genomic analyses were carried out. A phylogenomic tree was generated using the TYGS server, incorporating both isolates alongside type strains of closely related species (Fig. 1). This analysis revealed that strain S10 was clustered with *Citrobacter braakii* ATCC 51113 (i.e., originally isolated from a snake in France (Brenner et al. 1993)), with a digital DNA–DNA hybridization (dDDH) value of 90.7% (Table S1-A), exceeding the 70% threshold for species delineation. Similarly, strain DT1 grouped with *Acinetobacter calcoaceticus* DSM 30006 (i.e., isolated from a quinate-enriched soil in the Netherlands), with a dDDH value of 73.5% (Table S2-A). These taxonomic clusterings were further supported by pairwise Average Nucleotide Identity (ANI) analysis using the JSpeciesWS server (Fig. 2). Indeed, the ANI analysis revealed that S10 shared 99.04% ANI with *Citrobacter braakii* GTA-CB01 (Table S1-B), and DT1 showed 96.83% ANI with *Acinetobacter calcoaceticus* DSM 30006 (Table S2-B), both well above the species-level threshold of 95–96%. To further explore genomic conservation, a synteny analysis was conducted between the two genomes. Extensive collinear regions were observed (indicated by blue lines in Figure S3), indicating that large portions of the genome are organized in the same order and orientation. A smaller number of inverted regions (pink lines) were observed, indicating low levels of genomic rearrangements between strains (Fig. S3). Together, these results provide robust genomic evidence supporting the classification of S10 as *C. braakii* and DT1 as *A. calcoaceticus* and reveal high intra-genus genomic conservation within each lineage across diverse habitats.

Functional Genome Annotation of S10 and DT1

Genome annotations for both strains were performed using the RAST, COG, and KEGG databases. The total number of predicted genes was 4,774 and 3,818 for S10 and DT1, respectively. Of these, 4,693 genes in S10 and 3,663 in DT1 were functionally annotated by RAST, leaving 81 and 155 genes unannotated, respectively (Fig. S4). COG annotated 4,459 genes in S10 and 3,487 in DT1, while KEGG assigned functions to 3,365 and 2,010 genes, respectively. Classification assigned the annotated genes into 384 subsystems in S10 (Fig. 3a), and 310 subsystems in DT1 (Fig. 3b). In S10, the most enriched categories were carbohydrate metabolism (408 genes; 8.70%), followed by amino acids and derivatives (370 genes; 7.88%), protein metabolism (262 genes; 5.58%), and cofactors, vitamins, prosthetic groups, and pigments (181 genes; 3.86%). In DT1, the most abundant genes were associated with amino acids and derivatives (297 genes; 7.95%), followed by protein metabolism (200 genes; 5.36%), carbohydrate metabolism (160 genes; 4.28%), and cofactors, vitamins, prosthetic groups, and pigments (143 genes; 3.83%). According to COG functional classification, metabolism was the most dominant process in both genomes, encompassing 2,065 genes (45.06%) in S10 (Fig. 4a) and 1,518 genes (41.08%) in DT1 (Fig. 4b). Genes involved in cellular processes and signaling accounted for 23.16% of the genes in S10 and 16.82% in DT1, covering functions such as cell wall/membrane/envelope biogenesis, signal transduction, cell motility, post-translational modification, intracellular trafficking, secretion, vesicular transport and protein turnover. Interestingly, the S10 genome contains numerous flagellar biosynthesis genes (*e.g.*, *fliADEFGHIJKKMNOPQRST*, *flhABCDE*) (Table S4), in line with the motile nature of most *Citrobacter* species. In contrast, such genes were absent in the DT1 genome, consistent with the non-motile nature of *Acinetobacter* (Table S3). About 17% of coding sequences in both genomes were related to information storage and processing, encompassing functions such as translation, ribosomal structure and biogenesis, transcription, replication, recombination, and repair. A substantial fraction of genes was classified as having unknown functions, with 999 genes (21.80%) in the S10 genome and 1,115 genes (30.16%) in DT1. Finally, KEGG pathway mapping reinforced the dominance of metabolic genes, with 1,356 genes in S10 and 1,128 in DT1 assigned to metabolism-related pathways (Fig. 5). Additional prominent categories included environmental information processing (S10: 458 genes; DT1: 169), genetic information processing (S10: 222; DT1: 194), and cellular processes (S10: 259; DT1: 115).

Taken together, these annotations reveal that both genomes encode a broad repertoire of functional genes, with S10 showing greater metabolic diversity and DT1 exhibiting a higher proportion of genes with yet uncharacterized functions.

Genome mining for PGP and Stress-related genes

Functional genome comparison showed that both S10 and DT1 strains harbor a diverse repertoire of genes related to PGP traits, including auxin, cytokinin and siderophore biosynthesis, phosphate solubilization, nitrogen metabolism and ACC deaminase activity (Fig. 6, Table S3 and Table S4). Both strains carried gene clusters involved in IAA biosynthesis, notably *tyrB*, *trpABCDE*, and *ipdC*, a key gene in the indole-3-pyruvate (IPA) pathway. Genes related to cytokinin biosynthesis, *miaA*, *miaB*, and *miaE*, were also found in both genomes (Fig. 6). Interestingly, *aspC* (aspartate aminotransferase) was specific to the S10 genome, whereas *trpF* (N-(5'-phosphoribosyl) anthranilate isomerase) was identified only in DT1.

Although not directly involved in IAA biosynthesis, both genes contribute indirectly by supporting the availability of tryptophan, its primary precursor. In addition, key genes involved in the synthesis of riboflavin (vitamin B2) were also found in both the S10 and DT1 genomes, these include *ribA* (GTP cyclohydrolase II), *ribB* (3,4-dihydroxy-2-butanone 4-phosphate synthase), *ribD* (pyrimidine deaminase/reductase), *ribE* (lumazine synthase), and *ribC* (riboflavin synthase) (Fig. 6; Table S3; Table S4). These genes encode enzymes that convert one molecule of GTP and two molecules of ribulose-5-phosphate into one molecule of riboflavin, a crucial cofactor for plant metabolism, growth, and defense. Regarding phosphate solubilization, both genomes harbored the phosphate transporters gene *pstB* (Fig. 6), while *pstACS* genes were found only in S10 (Table S4). Core genes such as inorganic pyrophosphatase (*ppa*), exopolyphosphatase (*ppx*), polyphosphate kinase (*ppk*) and quinoprotein glucose dehydrogenase (*gcd*) were present in both strains. S10's genome encoded uniquely phosphonate, and carbon-phosphorus (C-P) lyases (*phnCDEGHIJK*), whereas additional genes involved in phosphate sensing and cofactor synthesis were found DT1, including phosphate regulon sensor protein (*phoR*), phosphate specific transport system accessory protein (*phoU*) and pyrroloquinoline synthase (*pqqG*). For nitrogen fixation, no complete nitrogenase gene cluster was identified in either genome, but nitrogen metabolism potential was evident. DT1 carried the *nirB* gene, encoding nitrite reductase catalytic subunit, while the S10 genome harbored a more extensive set of nitrate reduction genes, including the *narGHIVYZ* operon (Fig. 6, Table S3). Siderophore biosynthesis appeared to be under the control of several gene clusters, in S10 and DT1 genomes. Both strains carried genes for enterobactin (*entABCDEF*), and staphyloferrin B (*sbnABD*) biosynthesis. In addition, other siderophore-related genes including L-2,4-diaminobutyrate decarboxylase (*ddC*), diaminobutyrate-2-oxoglutarate aminotransferase (*dat*), 2,3-dihydroxybenzoate-AMP ligase (*dhbE*) were also identified, as well as genes related to iron storage (*bfr*) and transport (*feoABC*) (Fig. S6; Table S3; Table S4).

Finally, genes involved in ACC deaminase activity were detected. The S10 genome contained *rimI*, *rimK*, *rimL*, *rimM*, *rimO*, *rimP*, and *rimJ*, while DT1 carried *rimI*, *rimM*, *rimO*, and *rimP* (Fig. 6). These genes are involved in the degradation of 1-aminocyclopropane-1-carboxylate (ACC), the immediate precursor of ethylene, a plant hormone that inhibits growth under abiotic stress conditions (Shekhawat et al. 2022). Taken together, these findings demonstrate that S10 and DT1 harbor complementary and overlapping sets of genes involved in phytohormone biosynthesis, nutrient acquisition, stress mitigation, siderophore production and stress mitigation, supporting their functional potential as robust PGPR candidates for sustainable agriculture.

Genomic Analysis of Secondary Metabolism using AntiSMASH

To identify gene clusters involved in secondary metabolite synthesis in S10 and DT1, genome mining was performed using antiSMASH (version 8.). The analysis revealed that the S10 genome harbored two biosynthetic gene clusters (BGCs): one encoding a thiopeptide (O-antigen-related) and another

corresponding to an NRP-metallophore of the NRPS class, annotated as enterobactin (Table 3). In contrast, the DT1 genome harbored a broader diversity of secondary metabolite pathways, with eight predicted BGCs, including gene clusters for arylpolyenes, NI-siderophore, betalactone, redox-cofactor, NRP-metallophore, NRPS, and RiPP-like metabolites (Table 3). Comparison against the MIBiG reference database revealed varying degrees of similarity to characterized clusters. For instance, the enterobactin BGC from DT1 shared 55% similarity with a known orthologous cluster from *Pseudomonas sp.*, whereas the corresponding cluster in S10 exhibited full conservation (100%) with a reference Citrobacter cluster, suggesting potential divergence in siderophore structure, expression, or functionality between the two strains. Other BGCs in DT1 showed moderate similarity to clusters encoding APE VF, berninamycin variants, and mycosubtilin with 45%, 22%, and 20% similarity to clusters from *Aliivibrio fischeri* ES114, *Streptomyces* sp., and *Bacillus subtilis* subsp. *spizizenii* ATCC 6633, respectively. The remaining clusters showed less than 20% similarity to known BGCs, including 16% similarity with staphyloferrin B from *Staphylococcus aureus* subsp. *aureus* NCTC 8325, and 4% similarity with lagriene from *Burkholderia gladioli*. Altogether, these findings suggest that while S10 contains a limited set of conserved BGCs, DT1 exhibits a broader and more diverse secondary metabolite biosynthetic potential, likely reflecting an intrinsic genetic capacity for metabolic versatility, a trait commonly associated with microbial adaptability and survival in diverse or competitive environments (Dong et al. 2024).

Table 3

Biosynthetic gene clusters (BGCs) for secondary metabolites identified in the genome of *Acinetobacter calcoaceticus* DT1 and *Citrobacter braakii* S10. Gene cluster prediction was performed using antiSMASH v8.0 and annotations were cross-referenced with the MIBiG database.

Region	Type	From	To	Most similar know cluster	MIBIG Accession (% Gene Similarity)
***Acinetobacter calcoaceticus* DT1**					
1	NI-siderophore	1564594	1599021	staphyloferrin B*	BGC0000943 (16%)
2	redox-cofactor, NRP-metallophore, NRPS	1916080	2023816	Enterobactin*	BGC0000343 (55%)
3	betalactone	2367645	2396725	mycosubtilin	BGC0001103 (20%)
4	RiPP-like	2507421	2518284		
5	RiPP-like	2706268	2718466		
6	arylpolyene	2981396	3022625	berninamycin K/berninamycin J/berninamycin A/berninamycin B	BGC0002363 (22%)
7	arylpolyene	3321619	3365221	APE Vf	BGC0000837 (45%)
8	NRPS, hserlactone	3750029	3793988	lagriene	BGC0002455 (4%)
Citrobacter braakii S10					
1	Thiopeptide	3108899	3135189	O-antigen	BGC0000781 (14%)
2	NRP-metallophore, NRPS	3430326	3485411	Enterobactin	BGC0002476 (100%)

NRP non-ribosomal peptide, NRPS non-ribosomal peptide synthase.

* Genes associated with these clusters are presented in Fig. 6

Targeted and non-targeted metabolomic profiling of S10 and DT1 strains

Given the presence of genes involved in phytohormone biosynthesis (Fig. 6), we performed targeted metabolomic analysis using Liquid Chromatography–Q-Tandem Mass Spectrometry (LC-MS/MS) to assess the production of key metabolites in S10 and DT1. Both intracellular (cell pellet) and extracellular

(culture supernatant) fractions were analyzed to distinguish between metabolites synthesized in the bacteria and those actively or passively secreted into the environment, the latter being most relevant to plant-microbe interactions. This analysis confirmed the production of several phytohormones, including indole-3-acetic acid (IAA), D-abscisic acid, salicylic acid (SA), and the cytokinin 2-isopentenyladenine (Fig. 7). Among these, the most abundant hormone was IAA, especially in the supernatant of DT1 (confirming the data obtained in the assays using the Salkowski's reagent), indicating a high level of extracellular accumulation. In contrast, SA showed the lowest abundance in both supernatant and pellet fractions, but both strains produced comparable amounts of benzoic acid, a precursor of SA. Moreover, both strains produced equivalent amounts of riboflavin. Together with SA and benzoic acid, these metabolites are known to trigger both plant pathogen defense and abiotic stress tolerance (Azami-Sardooei et al. 2010; Senaratna et al. 2003).

To further explore the metabolic diversity of S10 and DT1, non-targeted metabolomic profiling was conducted using Liquid Chromatography-High-Resolution Tandem Mass Spectrometry with Quadrupole Time-of-Flight (LC–HRMS QTOF). Both pellet and supernatant fractions were analyzed, and metabolite annotation was performed using publicly available databases including NPA, KNApSAcK, PlantCyc, FoodDB, phenolExplorer, YMDB, ECMDB, and Spectral libraries.

To evaluate metabolic variations between intracellular and extracellular fractions of both strains, principal component analysis (PCA) was applied. The PCA score plot revealed a clear separation between the metabolic profiles of S10 and DT1, with the first principal component (PC1) accounting for 85.5% of the total variance (Fig. 8), indicating that strain identity is the main driver of metabolic differences. In contrast, the second principal component (PC2, 3% of the total variance) captured the subtler variation between intracellular and extracellular fractions, reflecting differences in metabolite accumulation and secretion.

Differential metabolite analysis (p-value < 0.05; fold change > 0,5|) identified 56 significantly different compounds between DT1 pellet and supernatant fractions. Among these, 45 were more abundant in the pellet (*e.g.*, N.N-Dimethyldodecylamine N-oxide, Guanine, Adenosine 3'-monophosphate, alpha-Linolenic acid and Farnesylacetone), while 11 were more abundant in the supernatant (*e.g.*, Perlolyrine, Radiosumin, Microcin SF608 and Maculosinin) (Table S5; Fig. 9a). In S10, 31 metabolites were differently identified between fractions, 20 were more abundant in the pellet and 11 in the supernatant (Table S6; Fig. 9a). Notably, no metabolites were shared among the differentially produced compounds in the supernatants of the two strains, whereas six metabolites were found in both pellets. Additionally, three overlaps were observed between the DT1 supernatants and the S10 pellet (Fig. 9b). Clustering heatmaps of differential metabolites for DT1 (Fig. 10a) and S10 (Fig. 11a) confirmed distinct metabolite distribution patterns between intracellular and extracellular compartments. KEGG pathway enrichment analysis revealed that the detected metabolites were significantly associated with pathways involved in plant secondary metabolites biosynthesis, amino acid metabolism, phytohormone production, and ABC transporter-mediated environmental signal sensing (Fig. 10b and 11b). Overall, targeted and untargeted metabolomic analyses confirmed the production of phytoactive and stress-related metabolites in both

strains, supporting their genomic potential and reinforcing their suitability as metabolically versatile PGPR candidates for plant health improvement.

Discussion

An increasing number of studies has emphasized the potential of PGPR to enhance plant health and productivity (Tripathi et al. 2024). In this context, we targeted the rhizosphere of two wild plant species, *Cynodon dactylon* and *Diplotaxis tenuifolia*, naturally thriving in arid environments, aiming to isolate bacterial strains potentially adapted to harsh conditions and endowed with PGP properties. From these rhizospheres, we isolated two strains, S10 and DT1, subsequently identified as *Citrobacter braakii* (S10) and *Acinetobacter calcoaceticus* (DT1), respectively. Although these species are best known for their opportunistic pathogenicity in clinical settings (Joly-Guillou 2005; Zhang et al. 2023), C. *braakii* has also been isolated from diverse environments including rhizospheric soil of rice grown in salt-affected areas (Nawaz et al. 2021).

PGPR promote plant growth and stress resilience by producing or modulating phytohormones such as auxins, gibberellins, and cytokinins, as well as regulating ethylene levels through ACC deaminase activity (Tripathi et al. 2024). To explore the PGP potential of S10 and DT1, we performed whole-genome annotation, focusing on pathways related to phytohormone biosynthesis and metabolism. Both genomes contain the tryptophan biosynthesis operon *trpABCDE*, a key pathway indirectly linked to indole-3-acetic acid (IAA) production, a major phytohormone involved in plant development (Babalola et al. 2021). Moreover, both strains harbor the *ipdC* gene, encoding indole-3-pyruvate (IPyA) decarboxylase, a key enzyme in the IPyA pathway of IAA biosynthesis (Jiang et al. 2023). The functional relevance of *ipdC* in PGP activity has been demonstrated by Figueredo et al. (2023), who reported that its inactivation in *Bacillus thuringiensis* RZ2MS9 markedly reduced the strain's capacity to promote maize growth. Consistent with these genomic findings, our targeted LC-MS/MS analysis confirmed substantial IAA production in both strains, particularly in the extracellular fraction of DT1 (Fig. 7). In addition to auxin production, S10 and DT1 also possess genes encoding ACC deaminase enzymes (*rimJ, rimK, rimL, rimM, rimO, rimP*, and *rimI*), which degrade 1-aminocyclopropane-1-carboxylate (ACC), the precursor of ethylene. By lowering ethylene levels, this activity helps mitigate growth inhibition under stress conditions such as drought and salinity, as observed in other PGPR including *Phytobacter palmae* WL65 (Thamvithayakorn et al. 2025).

Cytokinins (CK) also play a critical role in plant development by regulating cell division, shoot initiation, and photosynthesis (Gao et al. 2022). For instance, cytokinin production by *Rhizobium sp. WYJ-E13* promotes *Curcuma* root growth (Huang et al. 2022). In both S10 and DT1 genomes, we identified several genes involved in CK biosynthesis, including *miaABE* genes. These genes encode tRNA dimethylallyl transferases, which catalyze the biosynthesis of isopentenyladenosine (iPR), a key cytokinin precursor. Consistently, our targeted metabolomics confirmed the production of cytokinin 2-isopentenyladenine by

S10 and DT1. Similar CK biosynthesis genes were reported to be active in *Enterobacter mori* AYS9, where *miaA* and *miaB* are involved in converting iPR into biologically active cytokinins (Fadiji et al. 2023). The functional relevance of cytokinin biosynthesis in PGPR has also been demonstrated by Asif et al. (2022), who showed that these hormones protect photosynthetic pigments like carotenoids and chlorophylls. Consistently, *Priestia aryabhattai* and *Paenibacillus* sp. strains harboring *miaA* and *miaB* genes were reported to enhance chlorophyll content in tomato plants (Almirón et al. 2025).

Alongside cytokinins, riboflavin and its derivatives, flavin mononucleotide (FMN) and flavin adenine dinucleotide (FAD), are essential cofactors involved in photosynthesis, energy production, and redox metabolism (Sandoval et al. 2008). The beneficial impact of bacterial riboflavin production on plant health has been demonstrated by Ajeethan et al. (2023), who showed that inoculating kale seeds with *Sinorhizobium meliloti* 1021 (*i.e.*, a strain secreting significant amounts of flavins) led to significant improvements in growth compared to a flavin-deficient mutant. In our study, both S10 and DT1 genomes harbored genes for riboflavin biosynthesis, suggesting a role in supporting plant health. Combined with cytokinin biosynthesis genes, these results underscore the diverse metabolic strategies of S10 and DT1 in promoting plant growth under stress conditions. Building on this genomic evidence, our targeted metabolite profiling further revealed that both strains produce not only cytokinins and riboflavin, but also D-abscisic acid and salicylic acid. Similarly, *Priestia aryabhattai* and *Paenibacillus* sp. isolates from the tomato rhizosphere have been reported as PGPR capable of producing various phytohormones (Almirón et al. 2025). These findings underscore the multiple phytohormone-mediated mechanisms underlying the PGP potential of S10 and DT1.

Beyond targeted analyses, our comparative non-targeted metabolomic profiling revealed additional metabolites produced by S10 and DT1, with some accumulating differentially between intracellular and extracellular fractions (Figs. 10 and 11). Among these, cadaverine and biotin are known to enhance plant growth and stress tolerance (Jancewicz et al. 2016; Wang et al. 2020). Cadaverine has been linked to improved antioxidant defenses and tolerance to abiotic stresses (Gibbs et al. 2021; Ozmen et al. 2023). Biotin, another metabolite detected, supports plant development and resilience against carbonate stress (Wang et al. 2020). Notably, S10 produced arginine and trans-4-coumaric acid, compounds associated with photosynthetic enhancement and ROS signaling, respectively (Chen et al. 2022; Nkomo et al. 2019). DT1 produced indole-3-propionic acid (IPA), which promotes root development (Sun et al. 2024), as well as amino acids like valine, histidine, leucine, and proline, which support plant growth and stress adaptation (Ji et al. 2022; Liu et al. 2023; Renzetti et al. 2025; Sun et al. 2023). This strain also synthesized gamma-aminobutyric acid (GABA), known for enhancing tolerance to multiple stresses in plants (Golnari et al. 2021; Suhel et al. 2023). These diverse metabolites suggest significant potential for S10 and DT1 to promote plant growth and resilience under various environmental conditions. Notably, the co-production of plant-beneficial compounds such as phytohormones, riboflavin, siderophores, and polyamines like cadaverine may confer a broader functional capacity to modulate plant responses (Jancewicz et al. 2016; Olanrewaju et al. 2017; Vejan et al. 2016).

Siderophores sequester iron from the environment, reducing availability to phytopathogens and contributing to plant health (Zhang et al. 2020). Our analyses revealed numerous genes associated with siderophore production, including *entABCDEF, feoABC, dhbABCEF, efeBOU, sbnABD* (Fig. 6). AntiSMASH analysis identified clusters for enterobactin, bacillibactin, and staphyloferrin B, highlighting a broad siderophore biosynthetic capacity (Table 3; Table S3; Fig. S5). These clusters are linked to biocontrol and plant health in other species like *Bacillus amyloliquefaciens* (Dimopoulou et al., 2021), *Bacillus velezensis* (Zhang et al. 2024a; Zhang et al. 2024b) and *Methylobacterium aquaticum* (Juma et al. 2022).

Nitrogen fixation is a key PGPR trait enabling conversion of atmospheric nitrogen (N_2) into bioavailable forms (Masood et al. 2020). In our study, S10 and DT1 harbored the *nirB* gene, involved in nitrate reduction along with other nitrogen metabolism genes like *narGHI*. However, neither strain possessed the full nitrogenase cluster required for atmospheric nitrogen fixation, suggesting their role may be limited to nitrate assimilation rather than true nitrogen fixation (Guo et al. 2023).

Phosphorus-solubilizing bacteria (PSB) play a key role in mineralizing organic phosphorus and mobilizing inorganic phosphorus (Pan and Cai 2023). Previous studies have shown that S10 can solubilize organic phosphate *in vivo* (El Ifa et al. 2024). Our genomic data confirms that S10 carries genes like *gcd*, *phoARP*, *pstABCS*, and *pqqEFG* (Fig. 6), consistent with its phosphate-solubilizing phenotype. Importantly, we provide new evidence that DT1 also possesses genes associated with phosphate solubilization, suggesting its potential as a PSB. Consistently, both S10 and DT1 demonstrated functional activity *in vitro*, as evidenced by their ability to produce siderophore on CAS agar, solubilize phosphate, and grow on nitrogen-free media (Table 2; Fig. S1).

Together, these findings confirm the multifaceted PGP potential of S10 and DT1 and highlight their promise for application as bioinoculants in sustainable agriculture. In this context, a combined formulation of both strains may prove particularly effective, as it would leverage their complementary traits (*e.g.*, zinc solubilization by S10 and the broader metabolic repertoire of DT1) to maximize plant growth promotion across varied environmental conditions. This strategy, which harnesses the functional complementarity of compatible PGPR, warrants further testing under greenhouse and field conditions.

Conclusion

This study highlights the multifunctional plant growth-promoting potential of two rhizobacterial strains, *Citrobacter braakii* S10 and *Acinetobacter calcoaceticus* DT1 isolated from the rhizospheres of wild plants thriving in arid habitats. Comprehensive genomic and metabolomic analyses revealed diverse genes and metabolites associated with key PGP traits, including pathways for nitrogen fixation, phosphate and zinc solubilization, siderophore and phytohormone production, and stress resilience. These genomic insights were corroborated by phenotypic assays and metabolomic profiling, confirming the functional capabilities of both strains. The capacity of S10 and DT1 to produce a range of bioactive compounds underscores their adaptability and potential to support plant growth and stress tolerance under challenging conditions. Together, these findings provide a strong foundation for the future

application of these strains as bioinoculants in sustainable agriculture, offering eco-friendly alternatives to chemical fertilizers and supporting crop productivity in challenging environments. Future research should focus on evaluating their performance under greenhouse and field conditions to confirm their practical efficacy.

Declarations

Conflict of Interest

The authors declare no conflict of interest.

Funding

This work was funded by grants provided by the Tunisian Ministry of Higher Education and Scientific Research (MESRS) and the French Ministry of Europe and Foreign Affairs (MEAE) and Ministry of Higher Education and Research (MESR) under the project PHC Maghreb 23MAG09.

Author Contribution

Conceptualization, IG, AB, MH and CE.; methodology, IG, NS (PGPR traits), AB, AA, VC (genome assembly) CV, DH, JZ (metabolomic); validation, CE, AB, MH; formal analysis, IG, NS, AA, VC, CV (genome assembly, annotation, genome analysis), CV, DH, JZ (metabolomic); writing—original draft preparation, IG, CE, AB.; writing—review and editing, IG, AB, MH.,CE; visualization, IG, NS.; supervision, CE, AB.; funding acquisition, AB, CE, MH. All authors have read and agreed to the published version of the manuscript.

Acknowledgement

The authors thank Drs. Marie-Edith Chabouté and Etienne Herzog, IBMP-CNRS Strasbourg and Prof. Mustafa Barakate, Université Cadi Ayyad for their valuable advice.

Data Availability

Genome sequences have been submitted to NCBI database under the submission references SUB15592691 (Genome assembly of Citrobacter braakii S10) and SUB15592887 (Genome assembly of Acinetobacter calcoaceticus DT1).

References

1. Ajeethan N, Yurgel SN, Abbey L (2023) Role of Bacteria-Derived Flavins in Plant Growth Promotion and Phytochemical Accumulation in Leafy Vegetables. Int J Mol Sci 24(17). 10.3390/ijms241713311
2. Ajmal AW, Yasmin H, Hassan MN, Khan N, Jan BL, Mumtaz S (2022) Heavy Metal-Resistant Plant Growth-Promoting Citrobacter werkmanii Strain WWN1 and Enterobacter cloacae Strain JWM6 Enhance Wheat (Triticum aestivum L.) Growth by Modulating Physiological Attributes and Some Key Antioxidants Under Multi-Metal Stress. Front Microbiol 13:815704. 10.3389/fmicb.2022.815704
3. Almirón C, Petitti TD, Ponso MA, Romero AM, Areco VA, Bianco MI, Espariz M, Yaryura PM (2025) Functional and genomic analyses of plant growth promoting traits in Priestia aryabhattai and Paenibacillus sp. isolates from tomato rhizosphere. Sci Rep 15(1):3498. 10.1038/s41598-025-87390-0
4. Asif R, Yasmin R, Mustafa M, Ambreen A, Mazhar M, Rehman A, Ahmad M, Umbreen S (2022) Phytohormones as Plant Growth Regulators and Safe Protectors against Biotic and Abiotic Stress. In: Hano CFE (ed) Plant Hormones - Recent Advances, New Perspectives and Applications. IntechOpen, Rijeka. doi:10.5772/intechopen.102832
5. Azami-Sardooei Z, França SC, De Vleesschauwer D, Höfte M (2010) Riboflavin induces resistance against Botrytis cinerea in bean, but not in tomato, by priming for a hydrogen peroxide-fueled resistance response. Physiol Mol Plant Pathol 75(1):23–29. https://doi.org/10.1016/j.pmpp.2010.08.001
6. Aziz RK, Bartels D, Best AA, DeJongh M, Disz T, Edwards RA, Formsma K, Gerdes S, Glass EM, Kubal M, Meyer F, Olsen GJ, Olson R, Osterman AL, Overbeek RA, McNeil LK, Paarmann D, Paczian T, Parrello B, Pusch GD, Reich C, Stevens R, Vassieva O, Vonstein V, Wilke A, Zagnitko O (2008) The RAST Server: Rapid Annotations using Subsystems Technology. BMC Genomics 9(1):75. 10.1186/1471-2164-9-75
7. Babalola OO, Fasusi OA, Amoo AE, Ayangbenro AS (2021) Complete genome sequence of a plant growth-promoting rhizobacterium, Bacillus sp. strain OA1, isolated from soybeans. Biocatal Agric Biotechnol 36:102121. https://doi.org/10.1016/j.bcab.2021.102121
8. Brenner DJ, Grimont PA, Steigerwalt AG, Fanning GR, Ageron E, Riddle CF (1993) Classification of citrobacteria by DNA hybridization: designation of Citrobacter farmeri sp. nov., Citrobacter youngae sp. nov., Citrobacter braakii sp. nov., Citrobacter werkmanii sp. nov., Citrobacter sedlakii sp. nov., and three unnamed Citrobacter genomospecies. Int J Syst Bacteriol 43(4):645–658. 10.1099/00207713-43-4-645
9. Chen Q, Wang Y, Zhang Z, Liu X, Li C, Ma F (2022) Arginine Increases Tolerance to Nitrogen Deficiency in Malus hupehensis via Alterations in Photosynthetic Capacity and Amino Acids Metabolism. Frontiers in plant science 12–2021
10. Comeau D, Balthazar C, Novinscak A, Bouhamdani N, Joly DL, Filion M (2021) Interactions Between Bacillus Spp., Pseudomonas Spp. and Cannabis sativa Promote Plant Growth. Front Microbiol 12:715758. 10.3389/fmicb.2021.715758

11. De Coster W, Rademakers R (2023) NanoPack2: population-scale evaluation of long-read sequencing data. Bioinformatics 39(5). 10.1093/bioinformatics/btad311
12. Dong X, Zhang T, Wu W, Peng Y, Liu X, Han Y, Chen X, Gao Z, Xia J, Shao Z, Greening C (2024) A vast repertoire of secondary metabolites potentially influences community dynamics and biogeochemical processes in cold seeps. Sci Adv 10(17):eadl2281. 10.1126/sciadv.adl2281
13. El Ifa W, Belgaroui N, Sayahi N, Ghazala I, Hanin M (2024) Phytase-producing rhizobacteria enhance barley growth and phosphate nutrition. Front Sustainable Food Syst Volume 8–2024
14. Eswaran SUD, Sundaram L, Perveen K, Bukhari NA, Sayyed RZ (2024) Osmolyte-producing microbial biostimulants regulate the growth of Arachis hypogaea L. under drought stress. BMC Microbiol 24(1):165. 10.1186/s12866-024-03320-6
15. Fadiji AE, Ayangbenro AS, Babalola OO (2023) Draft Genome Sequence of Citrobacter freundii AYS58, a Potential Plant Growth-Promoting Endophyte. Microbiol Resour Announc 12(5):e0014223. 10.1128/mra.00142-23
16. Fanning S, Rogers L, Power K, Gaora P (2016) Escherichia coli and Other Enterobacteriaceae: Occurrence and Detection. Encyclopedia of Food and Health. 10.1016/B978-0-12-384947-2.00259-2
17. Figueredo EF, Cruz TAD, Almeida JR, Batista BD, Marcon J, Andrade PAM, Hayashibara CAA, Rosa MS, Azevedo JL, Quecine MC (2023) The key role of indole-3-acetic acid biosynthesis by Bacillus thuringiensis RZ2MS9 in promoting maize growth revealed by the ipdC gene knockout mediated by the CRISPR-Cas9 system. Microbiol Res 266:127218. 10.1016/j.micres.2022.127218
18. Gao B, Chai X, Huang Y, Wang X, Han Z, Xu X, Wu T, Zhang X, Wang Y (2022) Siderophore production in pseudomonas SP. strain SP3 enhances iron acquisition in apple rootstock. J Appl Microbiol 133(2):720–732. 10.1111/jam.15591
19. Gibbs NM, Su SH, Lopez-Nieves S, Mann S, Alban C, Maeda HA, Masson PH (2021) Cadaverine regulates biotin synthesis to modulate primary root growth in Arabidopsis. Plant J 107(5):1283–1298. 10.1111/tpj.15417
20. Golnari S, Vafaee Y, Nazari F, Ghaderi N (2021) Gamma-aminobutyric acid (GABA) and salinity impacts antioxidative response and expression of stress-related genes in strawberry cv. Aromas. Brazilian J Bot 44(3):639–651. 10.1007/s40415-021-00750-8
21. Guo K, Yang J, Yu N, Luo L, Wang E (2023) Biological nitrogen fixation in cereal crops: Progress, strategies, and perspectives. Plant Commun 4(2):100499. 10.1016/j.xplc.2022.100499
22. Gurevich A, Saveliev V, Vyahhi N, Tesler G (2013) QUAST: quality assessment tool for genome assemblies. Bioinformatics 29(8):1072–1075. 10.1093/bioinformatics/btt086
23. He D, Wan W (2021) Phosphate-Solubilizing Bacterium Acinetobacter pittii gp-1 Affects Rhizosphere Bacterial Community to Alleviate Soil Phosphorus Limitation for Growth of Soybean (Glycine max). Front Microbiol 12:737116. 10.3389/fmicb.2021.737116
24. Hu J, Fan J, Sun Z, Liu S (2020) NextPolish: a fast and efficient genome polishing tool for long-read assembly. Bioinformatics 36(7):2253–2255. 10.1093/bioinformatics/btz891

25. Hu J, Wang Z, Sun Z, Hu B, Ayoola AO, Liang F, Li J, Sandoval JR, Cooper DN, Ye K, Ruan J, Xiao CL, Wang D, Wu DD, Wang S (2024) NextDenovo: an efficient error correction and accurate assembly tool for noisy long reads. Genome Biol 25(1):107. 10.1186/s13059-024-03252-4
26. Huang X, Zeng Z, Chen Z, Tong X, Jiang J, He C, Xiang T (2022) Deciphering the potential of a plant growth promoting endophyte Rhizobium sp. WYJ-E13, and functional annotation of the genes involved in the metabolic pathway. Front Microbiol 13:1035167. 10.3389/fmicb.2022.1035167
27. Hunt M, Silva ND, Otto TD, Parkhill J, Keane JA, Harris SR (2015) Circlator: automated circularization of genome assemblies using long sequencing reads. Genome Biol 16:294. 10.1186/s13059-015-0849-0
28. Husna, Kim BE, Won MH, Jeong MI, Oh KK, Park DS (2023) Characterization and genomic insight of surfactin-producing Bacillus velezensis and its biocontrol potential against pathogenic contamination in lettuce hydroponics. Environ Sci Pollut Res Int 30(58):121487–121500. 10.1007/s11356-023-30871-4
29. Jancewicz AL, Gibbs NM, Masson PH (2016) Cadaverine's Functional Role in Plant Development and Environmental Response. Front Plant Sci 7:870. 10.3389/fpls.2016.00870
30. Ji H, Yang G, Zhang X, Zhong Q, Qi Y, Wu K, Shen T (2022) Regulation of salt tolerance in the roots of Zea mays by L-histidine through transcriptome analysis. Front Plant Sci Volume 13–2022
31. Jiang L, Seo J, Peng Y, Jeon D, Park SJ, Kim CY, Kim PI, Kim CH, Lee JH, Lee J (2023) Genome insights into the plant growth-promoting bacterium Saccharibacillus brassicae ATSA2(T). AMB Express 13(1):9. 10.1186/s13568-023-01514-1
32. Joly-Guillou ML (2005) Clinical impact and pathogenicity of Acinetobacter. Clin Microbiol Infect 11(11):868–873. 10.1111/j.1469-0691.2005.01227.x
33. Josephine CM, Thomas J (2021) Plant Growth Ameliorating and Rhizosphere Competent Native Acinetobacter pittii Strain F2 5 from the Rhizosphere of Zea mays L. Indian J Agricultural Res. 10.18805/IJARe.A-5822
34. Joshi H, Bisht N, Mishra S, Prasad V, Chauhan P (2023) Bacillus amyloliquefaciens Modulate Carbohydrate Metabolism in Rice-PGPR Cross-Talk Under Abiotic Stress and Phytohormone Treatments. J Plant Growth Regul 42:1–18. 10.1007/s00344-023-10913-4
35. Juma PO, Fujitani Y, Alessa O, Oyama T, Yurimoto H, Sakai Y, Tani A (2022) Siderophore for Lanthanide and Iron Uptake for Methylotrophy and Plant Growth Promotion in Methylobacterium aquaticum Strain 22A. Front Microbiol 13:921635. 10.3389/fmicb.2022.921635
36. Li ZJ, Tang SY, Gao HS, Ren JY, Xu PL, Dong WP, Zheng Y, Yang W, Yu YY, Guo JH, Luo YM, Niu DD, Jiang CH (2024) Plant growth-promoting rhizobacterium Bacillus cereus AR156 induced systemic resistance against multiple pathogens by priming of camalexin synthesis. Plant Cell Environ 47(1):337–353. 10.1111/pce.14729
37. Lin HR, Shu HY, Lin GH (2018) Biological roles of indole-3-acetic acid in Acinetobacter baumannii. Microbiol Res 216:30–39. 10.1016/j.micres.2018.08.004

38. Liu H, Su Y, Fan Y, Zuo D, Xu J, Liu Y, Mei X, Huang H, Yang M, Zhu S (2023) Exogenous leucine alleviates heat stress and improves saponin synthesis in Panax notoginseng by improving antioxidant capacity and maintaining metabolic homeostasis. Front Plant Sci Volume 14–2023
39. Mashabela MD, Tugizimana F, Steenkamp PA, Piater LA, Dubery IA, Terefe T, Mhlongo MI (2023) Metabolomic evaluation of PGPR defence priming in wheat (Triticum aestivum L.) cultivars infected with Puccinia striiformis f. sp. tritici (stripe rust). Front Plant Sci 14:1103413. 10.3389/fpls.2023.1103413
40. Masood S, Zhao XQ, Shen RF (2020) Bacillus pumilus promotes the growth and nitrogen uptake of tomato plants under nitrogen fertilization. Sci Hort 272:109581. https://doi.org/10.1016/j.scienta.2020.109581
41. Meier-Kolthoff JP, Göker M (2019) TYGS is an automated high-throughput platform for state-of-the-art genome-based taxonomy. Nat Commun 10(1):2182. 10.1038/s41467-019-10210-3
42. Mhlongo MI, Piater LA, Dubery IA (2022) Profiling of Volatile Organic Compounds from Four Plant Growth-Promoting Rhizobacteria by SPME-GC-MS: A Metabolomics Study. Metabolites 12(8). 10.3390/metabo12080763
43. Mmotla K, Sibanyoni NR, Allie F, Sitole L, Mafuna T, Mashabela MD, Mhlongo MI (2025) Exploring the intricacies of plant growth promoting rhizobacteria interactions: an omics review. Ann Microbiol 75(1):5. 10.1186/s13213-025-01793-y
44. Moriya Y, Itoh M, Okuda S, Yoshizawa AC, Kanehisa M (2007) KAAS: an automatic genome annotation and pathway reconstruction server. Nucleic Acids Res 35(suppl2):W182–W185. 10.1093/nar/gkm321
45. Mujumdar S, Bhoyar J, Akkar A, Hundekar S, Agnihotri N, Jaybhay P, Bhuyan S (2023) Chap. 15 - Acinetobacter: A versatile plant growth-promoting rhizobacteria (PGPR). In: Swapnil P, Meena M, Harish, Marwal A, Vijayalakshmi S, Zehra A (eds) Plant-Microbe Interaction - Recent Advances in Molecular and Biochemical Approaches. Academic Press, pp 327–362. https://doi.org/10.1016/B978-0-323-91875-6.00009-8
46. Nawaz A, Mubeen F, Qamar ZU, Marghoob MU, Aziz S, Gross H (2021) Draft Genome Sequence of the Halophilic Strain Citrobacter braakii AN-PRR1, Isolated from Rhizospheric Soil of Rice (Oryza sativa L.) from Pakistan. Microbiol Resour Announc 10(38):e0078721. 10.1128/MRA.00787-21
47. Nkomo M, Gokul A, Keyster M, Klein A (2019) Exogenous p-Coumaric Acid Improves Salvia hispanica L. Seedl Shoot Growth Plants 8(12). 10.3390/plants8120546
48. Okla MK, Javed S, Tahir MF, Anas M, Saleem MH, Ahmed T, Saleh IA, Zomot N, Alwasel YA, Abdel-Maksoud MA, Ali S, Fahad S (2025) Evaluating the potential of Acinetobacter calcoaceticus in alleviation of aluminium stress in Triticum aestivum. 3 Biotech 15(1):34. 10.1007/s13205-024-04192-3
49. Olanrewaju OS, Glick BR, Babalola OO (2017) Mechanisms of action of plant growth promoting bacteria. World J Microbiol Biotechnol 33(11):197. 10.1007/s11274-017-2364-9

50. Ozmen S, Tabur S, Oney-Birol S (2023) Alleviation role of exogenous cadaverine on cell cycle, endogenous polyamines amounts and biochemical enzyme changes in barley seedlings under drought stress. Sci Rep 13(1):17488. 10.1038/s41598-023-44795-z
51. Pan L, Cai B (2023) Phosphate-Solubilizing Bacteria: Advances in Their Physiology, Molecular Mechanisms and Microbial Community Effects. Microorganisms 11(12). 10.3390/microorganisms11122904
52. Parks DH, Imelfort M, Skennerton CT, Hugenholtz P, Tyson GW (2015) CheckM: assessing the quality of microbial genomes recovered from isolates, single cells, and metagenomes. Genome Res 25(7):1043–1055. 10.1101/gr.186072.114
53. Paterson J, Jahanshah G, Li Y, Wang Q, Mehnaz S, Gross H (2017) The contribution of genome mining strategies to the understanding of active principles of PGPR strains. FEMS Microbiol Ecol 93(3):fiw249. doi.org/10.1093/femsec/fiw249
54. Pikovskaya R (1948) Mobilization of Phosphorus in Soil in Connection with the Vital Activity of Some Microbial Species—ScienceOpen
55. Renzetti M, Funck D, Trovato M (2025) Proline and ROS: A Unified Mechanism in Plant Development and Stress Response? Plants 14(1). 10.3390/plants14010002
56. Richter M, Rossello-Mora R, Glöckner F, Peplies J (2015) JSpeciesWS: A web server for prokaryotic species circumscription based on pairwise genome comparison. Bioinformatics 32. 10.1093/bioinformatics/btv681
57. Sandoval FJ, Zhang Y, Roje S (2008) Flavin nucleotide metabolism in plants: monofunctional enzymes synthesize fad in plastids. J Biol Chem 283(45):30890–30900. 10.1074/jbc.M803416200
58. Saravanan VS, Kalaiarasan P, Madhaiyan M, Thangaraju M (2007) Solubilization of insoluble zinc compounds by Gluconacetobacter diazotrophicus and the detrimental action of zinc ion (Zn2+) and zinc chelates on root knot nematode Meloidogyne incognita. Lett Appl Microbiol 44(3):235–241. 10.1111/j.1472-765X.2006.02079.x
59. Sayahi N, Djemal R, Ben Merdes K, Saidii MN, Yengui M, Gdoura R, Ebel C, Aydi S, Mechichi T, Hanin M (2022) Characterization of Siccibacter sp. Strain C2 a Novel Rhizobacterium that Enhances Tolerance of Barley to Salt Stress. Curr Microbiol 79(8):239. 10.1007/s00284-022-02930-5
60. Schwyn B, Neilands JB (1987) Universal chemical assay for the detection and determination of siderophores. Anal Biochem 160(1):47–56. 10.1016/0003-2697(87)90612-9
61. Seemann T (2014) Prokka: rapid prokaryotic genome annotation. Bioinformatics 30(14):2068–2069. 10.1093/bioinformatics/btu153
62. Senaratna T, Merritt D, Dixon K, Bunn E, Touchell D, Sivasithamparam K (2003) Benzoic acid may act as the functional group in salicylic acid and derivatives in the induction of multiple stress tolerance in plants. Plant Growth Regul 39:77–81. 10.1023/A:1021865029762
63. Shekhawat K, Frohlich K, Garcia-Ramirez GX, Trapp MA, Hirt H (2022) Ethylene: A Master Regulator of Plant-Microbe Interactions under Abiotic Stresses. Cells 12(1). 10.3390/cells12010031

64. Siddikee MA, Chauhan PS, Anandham R, Han GH, Sa T (2010) Isolation, characterization, and use for plant growth promotion under salt stress, of ACC deaminase-producing halotolerant bacteria derived from coastal soil. J Microbiol Biotechnol 20(11):1577–1584. 10.4014/jmb.1007.07011
65. Sobarzo J, Jorquera M, Martínez O, Menezes-Blackburn D, Fernández MT, Marschner P, Greiner R, Mora ML (2013) Indole acetic acid and phytase activity produced by rhizosphere bacilli as affected by pH and metals. J Soil Sci Plant Nutr 11:1–12. 10.4067/S0718-95162011000300001
66. Suhel M, Husain T, Prasad SM, Singh VP (2023) GABA Requires Nitric Oxide for Alleviating Arsenate Stress in Tomato and Brinjal Seedlings. J Plant Growth Regul 42(2):670–683. 10.1007/s00344-022-10576-7
67. Sun M, Li S, Yu H, Gong Q, Zhang B, Liu G, Xiao Y, Peng F (2023) Effects of Valine and Urea on Carbon and Nitrogen Accumulation and Lignin Content in Peach Trees. Plants 12(8). 10.3390/plants12081596
68. Sun W, Shahrajabian MH, Wang N (2025) A Study of the Different Strains of the Genus Azospirillum spp. on Increasing Productivity and Stress Resilience in Plants. Plants (Basel) 14(2). 10.3390/plants14020267
69. Sun Y, Yang Z, Zhang C, Xia J, Li Y, Liu X, Sun L, Tan S (2024) Indole-3-propionic acid regulates lateral root development by targeting auxin signaling in Arabidopsis. iScience 27(7):110363. 10.1016/j.isci.2024.110363
70. Thamvithayakorn P, Phosri C, Vishal V, Suwannasai N (2025) Characterization and Whole-Genome Sequencing of Phytobacter palmae WL65, a Plant Growth-Promoting Rhizobacterium First Isolated from Rice Rhizosphere Soil in Thailand. Agriculture 15(7). 10.3390/agriculture15070707
71. Tripathi A, Pandey VK, Jain D, Singh G, Brar NS, Taufeeq A, Pandey I, Dash KK, Samrot AV, Rustagi S (2024) An updated review on significance of PGPR-induced plant signalling and stress management in advancing sustainable agriculture. J Agric Food Res 16:101169. https://doi.org/10.1016/j.jafr.2024.101169
72. Vallenet D, Calteau A, Dubois M, Amours P, Bazin A, Beuvin M, Burlot L, Bussell X, Fouteau S, Gautreau G, Lajus A, Langlois J, Planel R, Roche D, Rollin J, Rouy Z, Sabatet V, Médigue C (2020) MicroScope: an integrated platform for the annotation and exploration of microbial gene functions through genomic, pangenomic and metabolic comparative analysis. Nucleic Acids Res 48(D1):D579–d589. 10.1093/nar/gkz926
73. Vejan P, Abdullah R, Khadiran T, Ismail S, Nasrulhaq Boyce A (2016) Role of Plant Growth Promoting Rhizobacteria in Agricultural Sustainability-A Review. Molecules 21(5). 10.3390/molecules21050573
74. Wang Y, Wang M, Ye X, Liu H, Takano T, Tsugama D, Liu S, Bu Y (2020) Biotin plays an important role in Arabidopsis thaliana seedlings under carbonate stress. Plant Sci 300:110639. 10.1016/j.plantsci.2020.110639
75. Wick RR, Judd LM, Holt KE (2019) Performance of neural network basecalling tools for Oxford Nanopore sequencing. Genome Biol 20(1):129. 10.1186/s13059-019-1727-y

76. Wood DE, Lu J, Langmead B (2019) Improved metagenomic analysis with Kraken 2. Genome Biol 20(1):257. 10.1186/s13059-019-1891-0
77. Wu L, Ding X, Lin Y, Lu X, Lv H, Zhao M, Yu R (2022) Nitrogen removal by a novel heterotrophic nitrification and aerobic denitrification bacterium Acinetobacter calcoaceticus TY1 under low temperatures. Bioresour Technol 353:127148. 10.1016/j.biortech.2022.127148
78. Zafar-ul-Hye M, Danish S, Abbas M, Ahmad M, Munir TM (2019) ACC Deaminase Producing PGPR Bacillus amyloliquefaciens and Agrobacterium fabrum along with Biochar Improve Wheat Productivity under Drought Stress. Agronomy 9(7). 10.3390/agronomy9070343
79. Zhang G, Zhao Q, Ye K, Ye L, Ma Y, Yang J (2023) Molecular analysis of clinical Citrobacter spp. isolates: Acquisition of the Yersinia high-pathogenicity island mediated by ICEkp in C. freundii. Front Microbiol 14:1056790. 10.3389/fmicb.2023.1056790
80. Zhang L, Zhang W, Li Q, Cui R, Wang Z, Wang Y, Zhang YZ, Ding W, Shen X (2020) Deciphering the Root Endosphere Microbiome of the Desert Plant Alhagi sparsifolia for Drought Resistance-Promoting Bacteria. Appl Environ Microbiol 86(11). 10.1128/AEM.02863-19
81. Zhang T, Jian Q, Yao X, Guan L, Li L, Liu F, Zhang C, Li D, Tang H, Lu L (2024a) Plant growth-promoting rhizobacteria (PGPR) improve the growth and quality of several crops. Heliyon 10(10):e31553. https://doi.org/10.1016/j.heliyon.2024.e31553
82. Zhang X, Xin Y, Wang J, Dhanasekaran S, Yue Q, Feng F, Gu X, Li B, Zhao L, Zhang H (2024b) Characterization of a Bacillus velezensis strain as a potential biocontrol agent against soft rot of eggplant fruits. Int J Food Microbiol 410:110480. https://doi.org/10.1016/j.ijfoodmicro.2023.110480

Figures

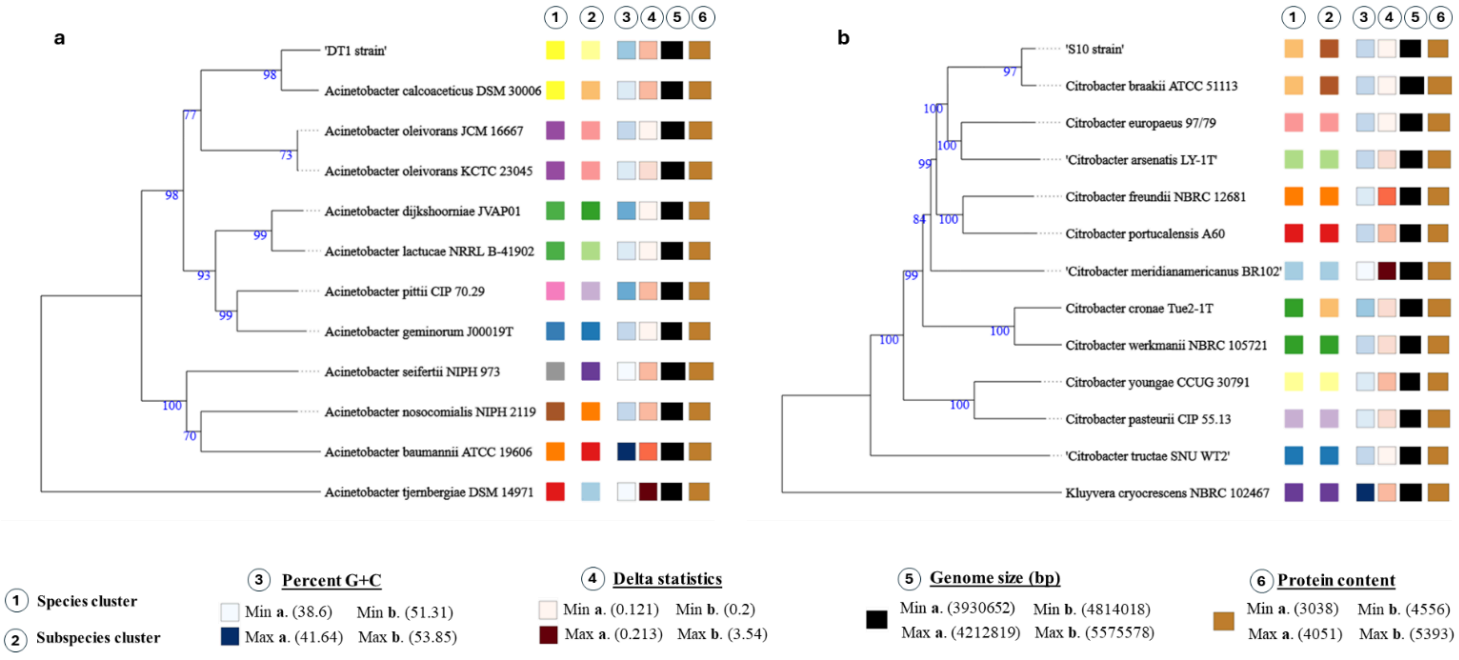

Figure 1

Genome-based phylogenetic positioning of *Acinetobacter calcoaceticus* DT1 and *Citrobacter braakii* S10. Phylogenetic tree of DT1 (**a**) and S10 (**b**) inferred using FastME 2.1.6.1 from Genome BLAST Distance Phylogeny (GBDP) calculated from whole-genome sequences. Branch lengths are scaled according to the GBDP distance formula d5. Pseudo-bootstrap support values (> 60 %) are shown above branches and were calculated from 100 replicates, with an average branch support of 89.7 %. The trees are midpoint-rooted. The colored and/or scaled squares to the right of each taxon correspond to six genomic or taxonomic features, indexed as follows: 1. Species cluster (color-coded); 2. Subspecies cluster (color-coded); 3. G+C content (blue gradient : light blue = low, dark blue = high); 4. Delta statistics (brown gradient: darker squares = higher deviation from tree-likeness); 5. Genome size (square size proportional to total genome length); Protein-coding gene content (square size proportional to number of CDS). Strains DT1 and S10 are highlighted at the top of their respective trees and compared to reference genomes within the *Acinetobacter* and *Citrobacter* genera.

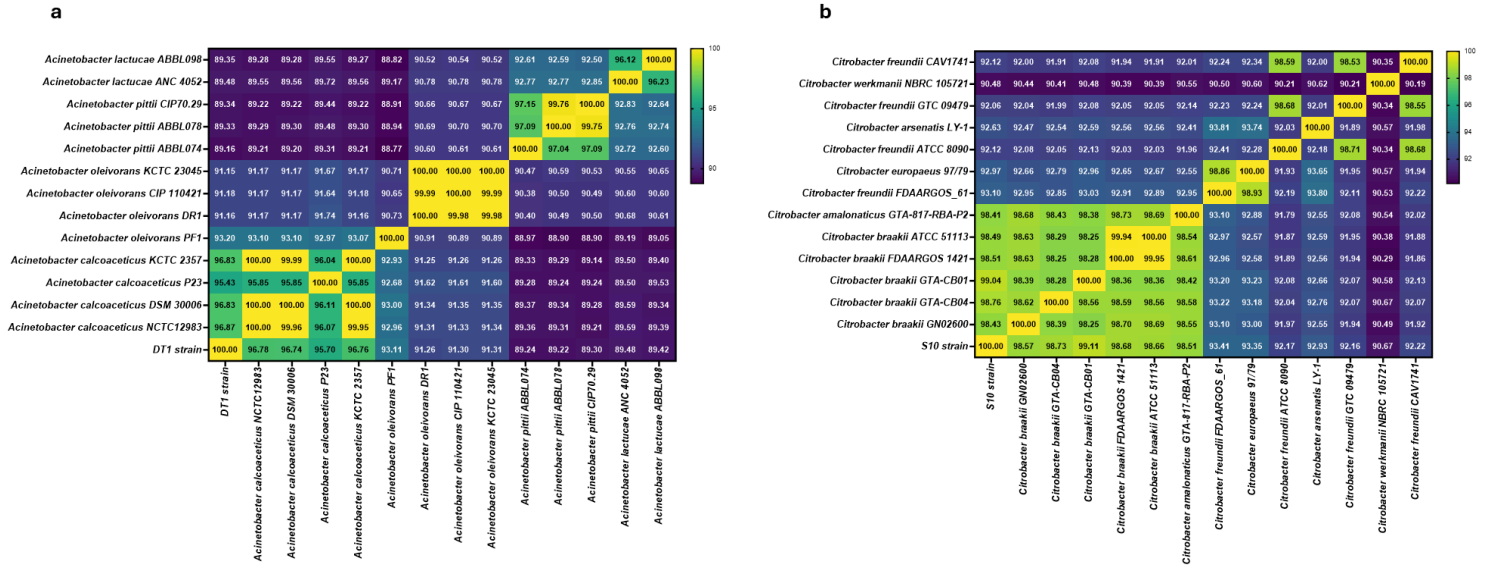

Figure 2

Average Nucleotide Identity (ANI) heatmaps of *Acinetobacter calcoaceticus* DT1 and *Citrobacter braakii* S10. ANI-based comparisons were performed to assess the genomic similarity of strain DT1 (**a**) with 13 *Acinetobacter* reference genomes, and strain S10 (**b**) with 13 *Citrobacter* genomes. Pairwise ANI values are visualized as heatmaps, where colors indicate percent identity at the nucleotide level. The gradient ranges from blue (low similarity) to yellow (high similarity), as shown in the accompanying color scale. These analyses were conducted using the JSpeciesWS server, with species-level boundaries typically considered at 95–96% ANI.

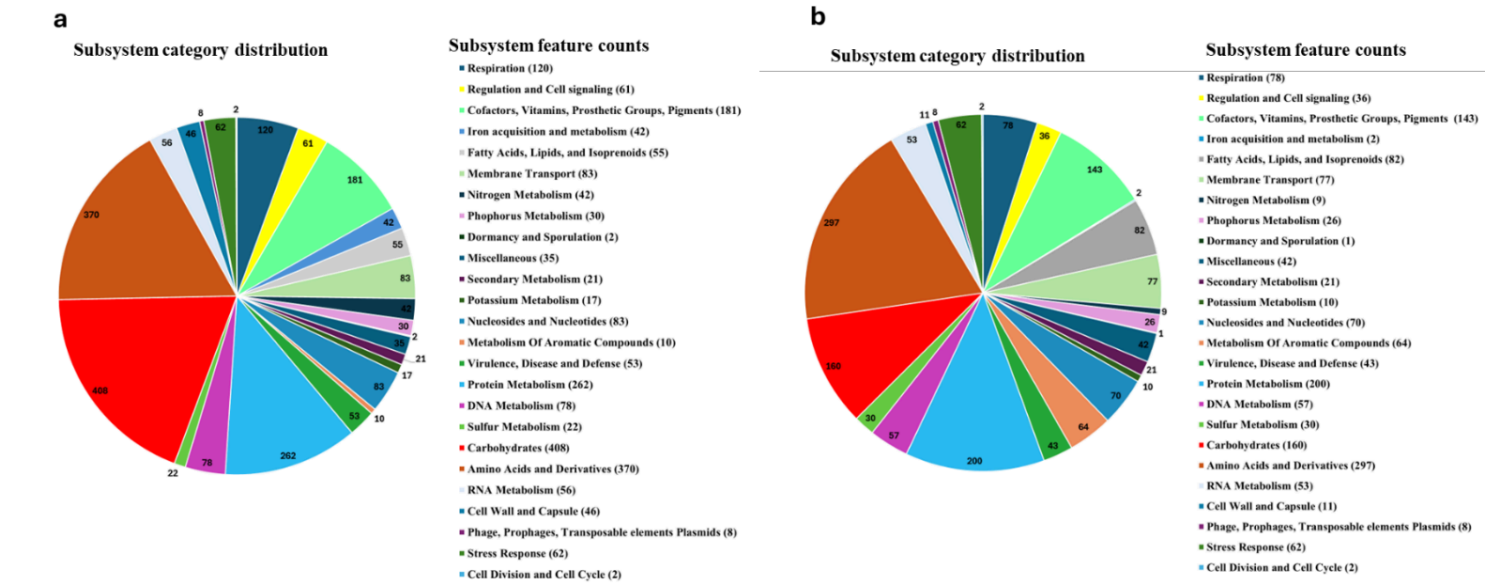

Figure 3

Functional subsystem category distribution in the genomes of *Citrobacter braakii* S10 and *Acinetobacter calcoaceticus* DT1. were annotated using the RAST server and are grouped by major biological processes. The number of genes assigned to each subsystem is shown for S10 (**a**) and DT1 (**b**). Categories include core metabolic processes such as carbohydrate metabolism, amino acid synthesis, stress response, and cofactor production. Annotations were generated using RAST (Rapid Annotations using Subsystems Technology; accessed via https://rast.nmpdr.org).

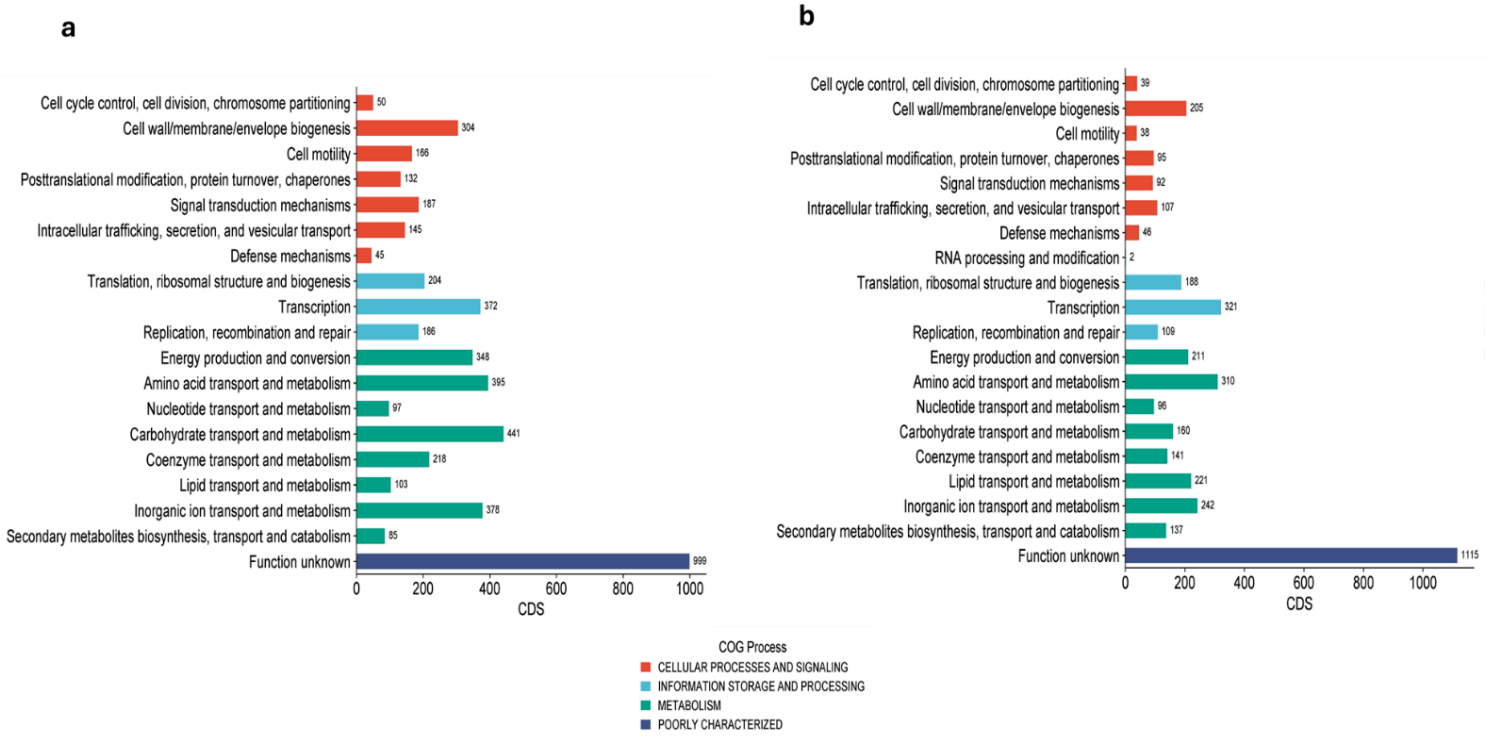

Figure 4

COG-based functional annotation of *Citrobacter braakii* S10 and *Acinetobacter calcoaceticus* DT1 genomes. Predicted protein-coding genes from S10 (**a**) and DT1 (**b**) were classified into Clusters of Orthologous Groups (COG) functional categories. Each bar represents the number of genes assigned to a specific functional group, reflecting major cellular processes, metabolism, and information storage and processing. Annotations were obtained using the COG database via the MicroScope platform (https://mage.genoscope.cns.fr/microscope).

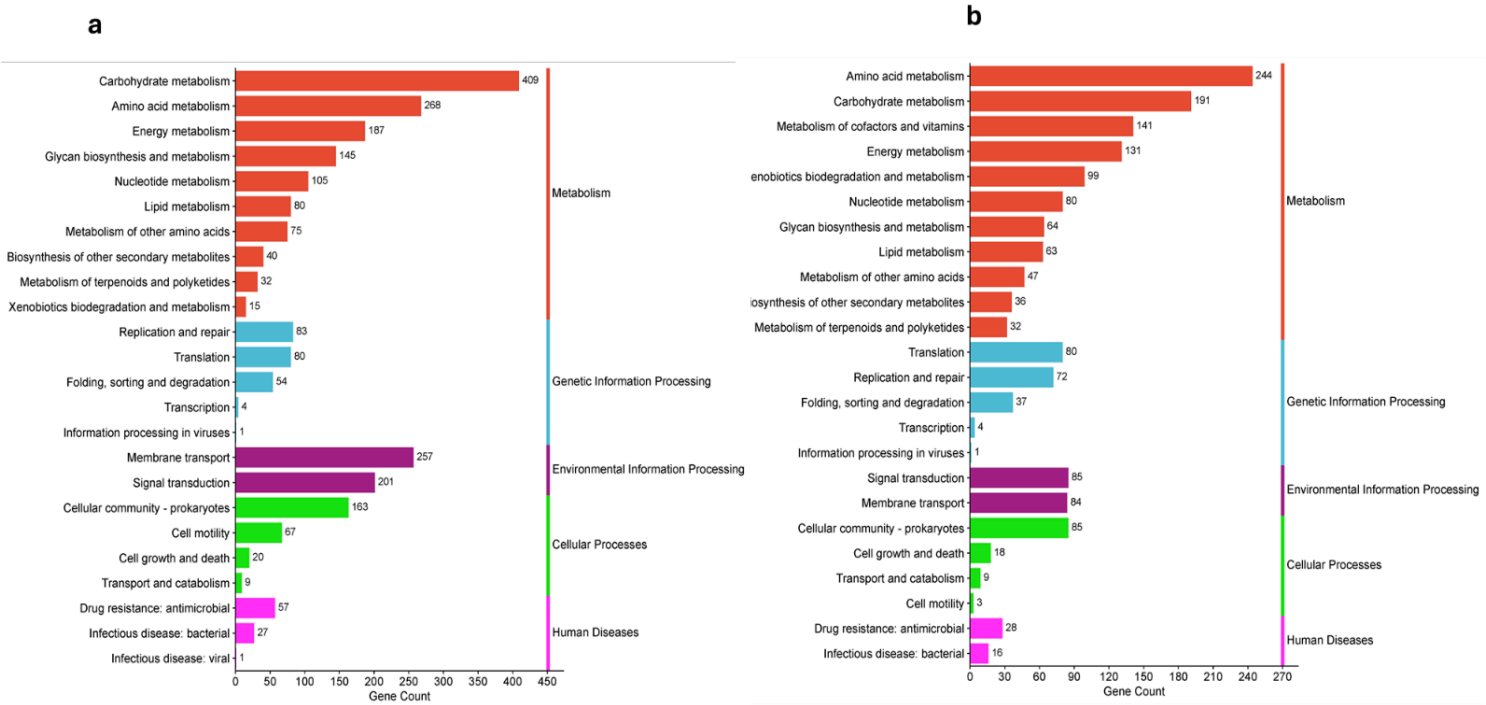

Figure 5

KEGG-based functional classification of genes in *Citrobacter braakii* S10 and *Acinetobacter calcoaceticus* DT1 genomes. Functional annotation results of KEGG database of *Citrobacter braakii S10* genome (a) and *Acinetobacter calcoaceticus* DT1 (b). The identified genes were classified into five major KEGG pathway categories: Metabolism, Genetic Information Processing, Environmental Information Processing, Cellular Processes, and Human Diseases. The bar plots reflect the number of genes assigned to each category, highlighting the predominance of metabolic and environmental processing functions in both strains.

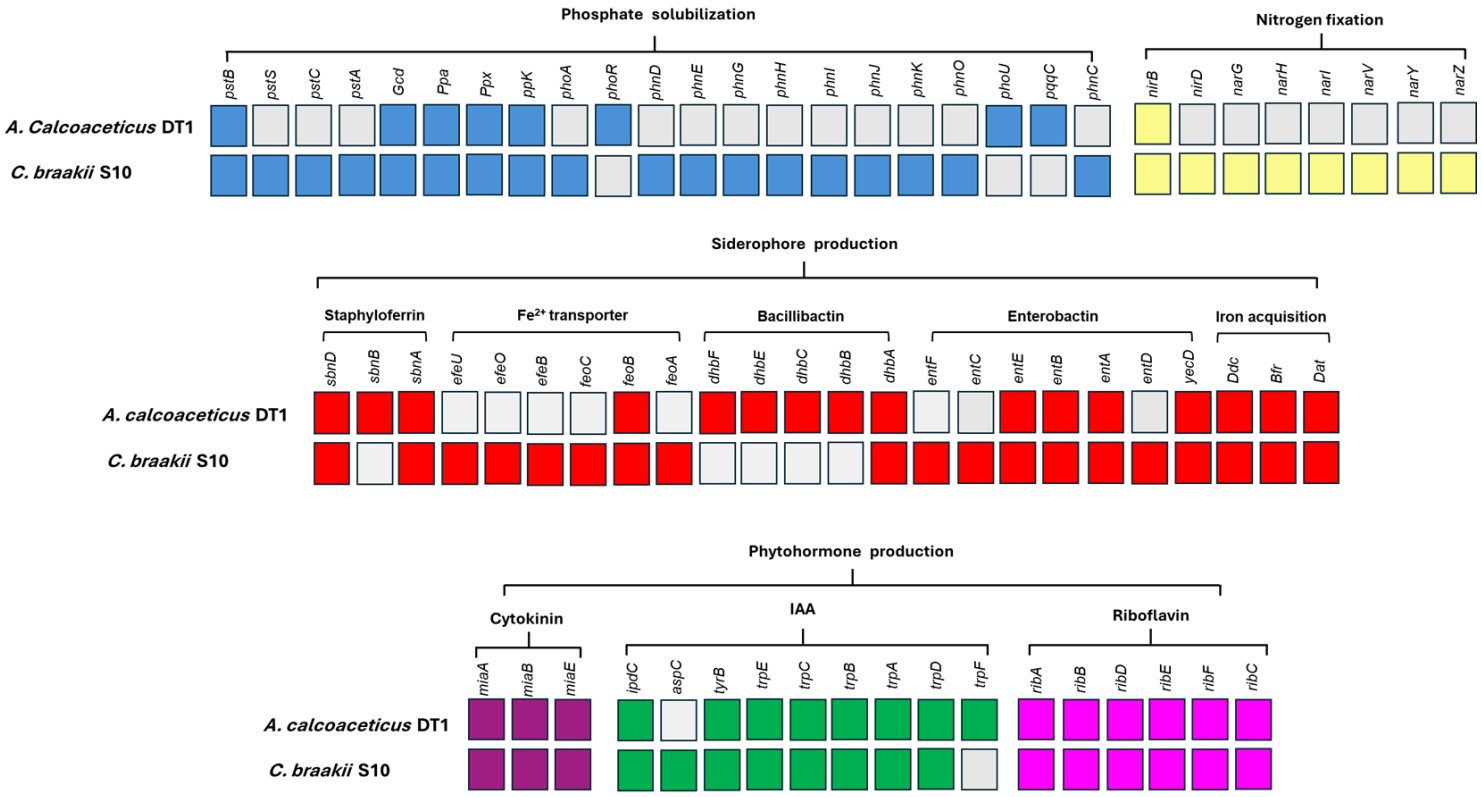

Figure 6

Distribution of genes related to plant growth-promoting (PGP) traits in *Acinetobacter calcoaceticus* DT1 and *Citrobacter braakii* S10. This presence/absence matrix summarizes key functional genes associated with PGP activities, including phytohormone biosynthesis, phosphate solubilization, nitrogen metabolism, siderophore production, and stress resilience. Colored boxes indicate the presence of a given gene in the genome, while white boxes indicate its absence. The comparison highlights both shared and strain-specific genetic determinants supporting plant growth promotion.

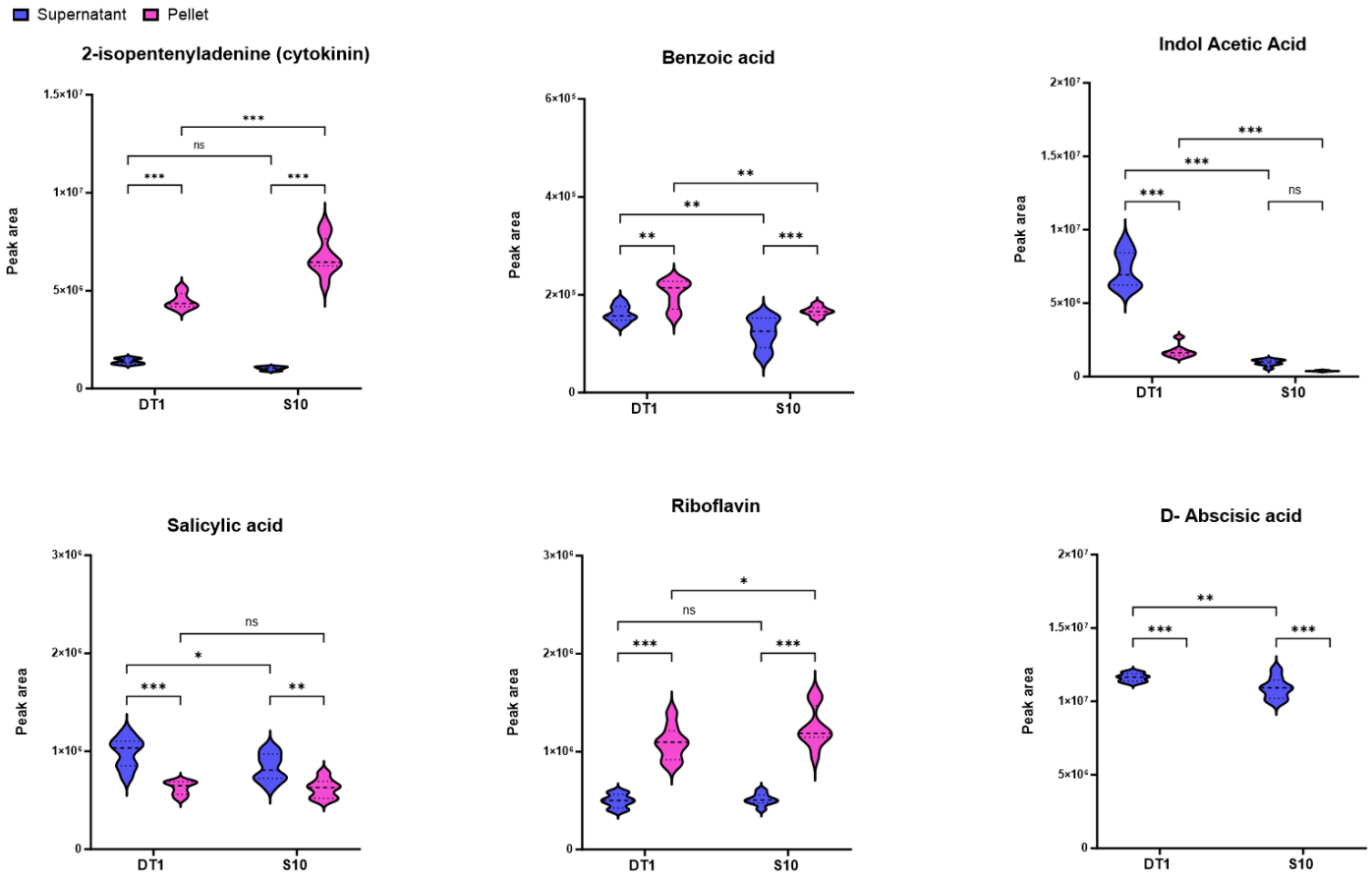

Figure 7

Quantification of phytohormones in *Citrobacter braakii* S10 and *Acinetobacter calcoaceticus* DT1 strains. Targeted metabolomic profiling was conducted using Liquid Chromatography–Q-Tandem Mass Spectrometry (LC-MS/MS) to quantify phytohormones in both extracellular (supernatant) and intracellular (pellet) fractions of bacterial cultures. Violin plots show the signal intensities of indole-3-acetic acid (IAA), D-abscisic acid, salicylic acid (SA), and 2-isopentenyladenine (2-iP) for each strain.

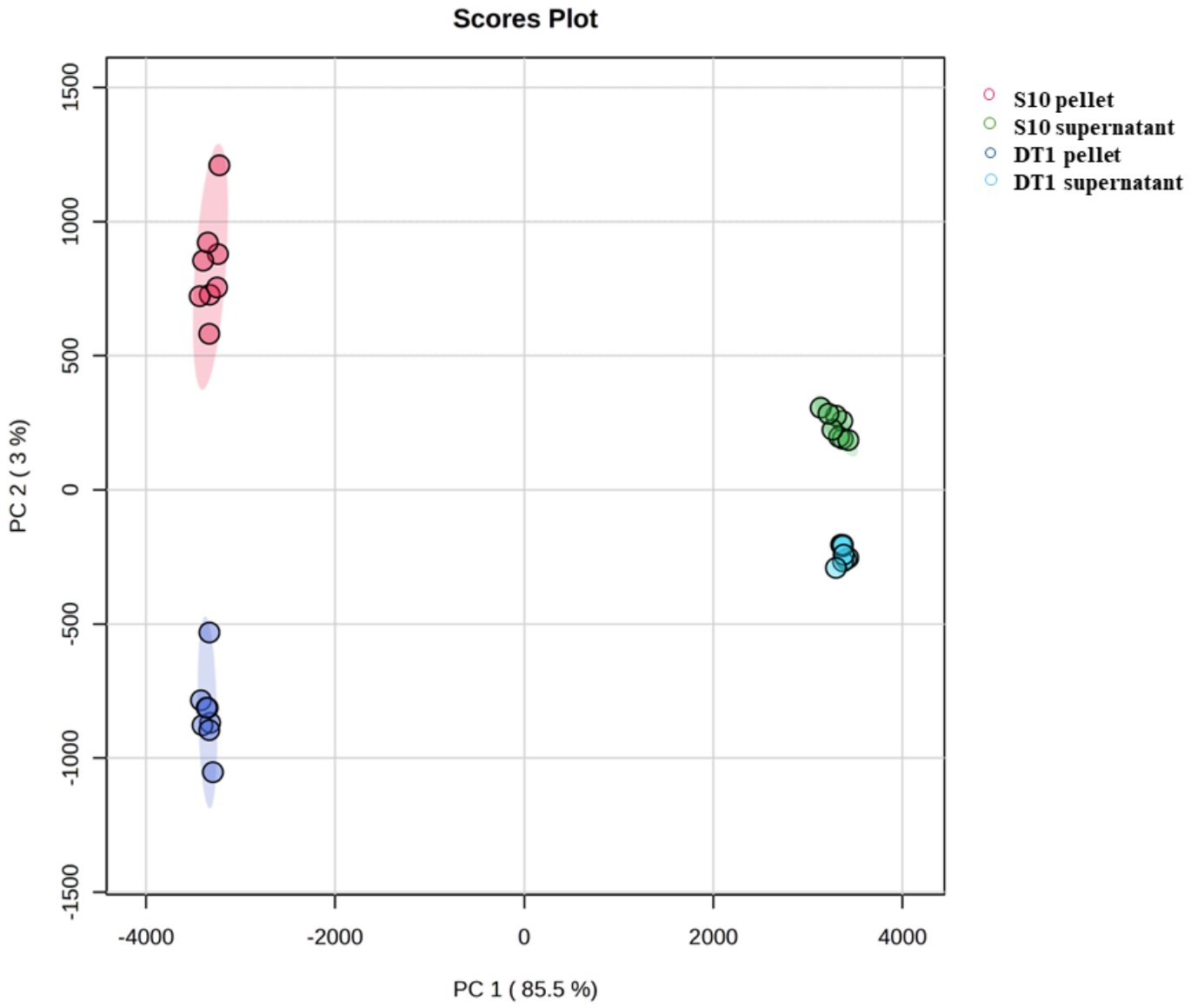

Figure 8

Principal Component Analysis (PCA) of the global metabolic profiles of *Citrobacter braakii* S10 and *Acinetobacter calcoaceticus* DT1. Non-targeted metabolomic profiling was performed on intracellular (pellet) and extracellular (supernatant) fractions using Liquid Chromatography–High-Resolution Mass Spectrometry coupled with Quadrupole Time-of-Flight (LC–HRMS QTOF). PCA was computed using MetaboAnalyst 5.0 to visualize global metabolic differences between strains and sample types. Each point represents one replicate of intracellular or extracellular metabolite profile.

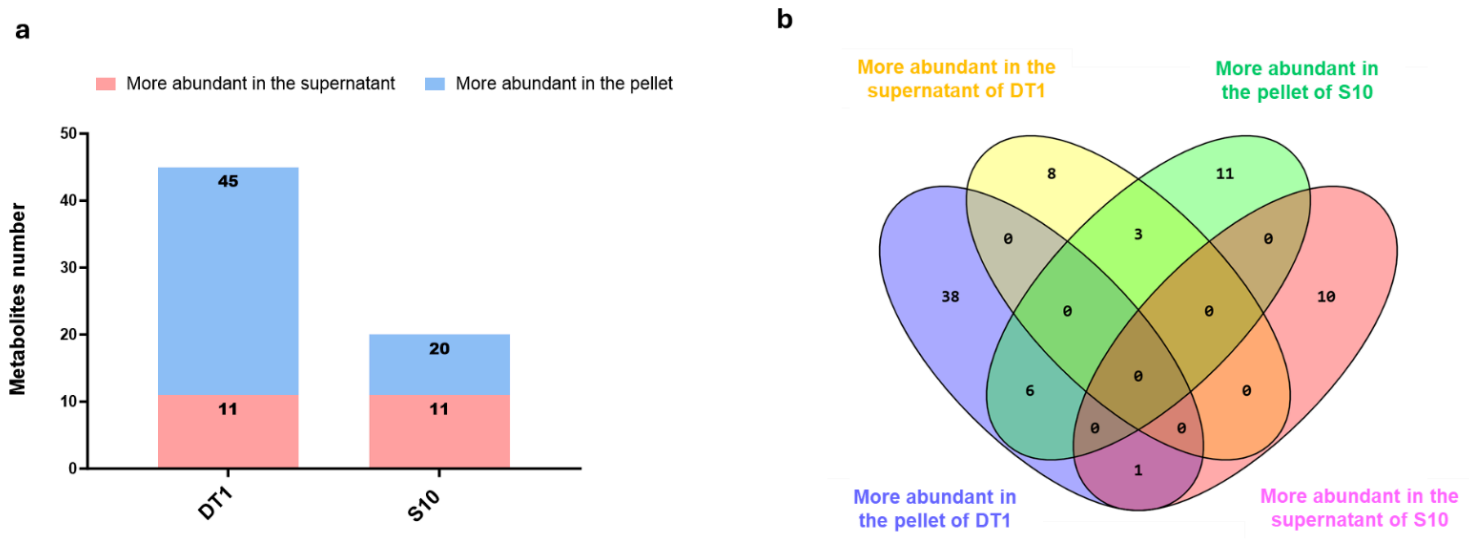

Figure 9

Differential metabolite abundance and overlap between *Citrobacter braakii* S10 and *Acinetobacter calcoaceticus* DT1. (**a**) Stacked bar chart showing the number of significantly more abundant (blue) and less abundant (pink) metabolites identified in the intracellular (pellet) fractions of S10 and DT1 strains, based on LC–HRMS QTOF non-targeted metabolomics and statistical thresholds (fold change > |0,5|; $p < 0.05$). (**b**) Four-way Venn diagram illustrating the overlap of differentially abundant metabolites between pellet and supernatant of the two strains.

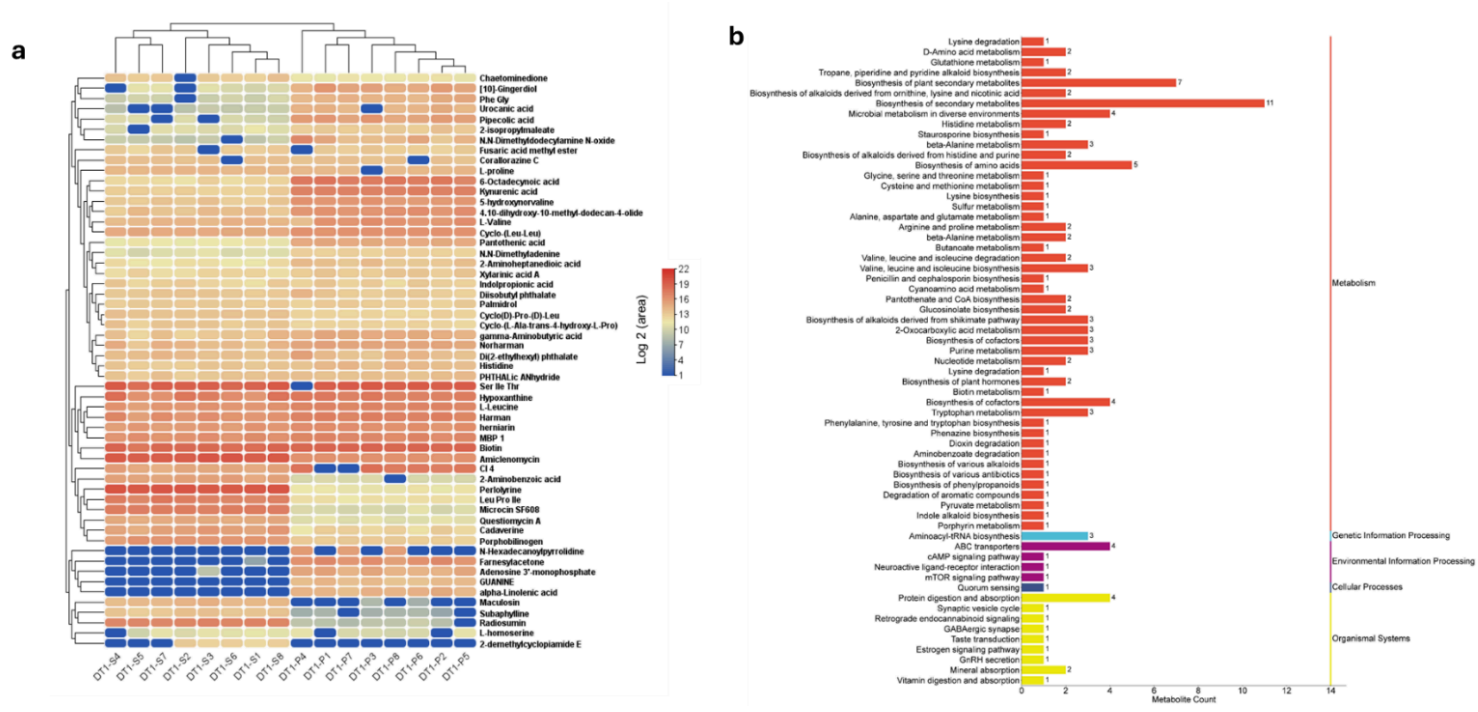

Figure 10

Intracellular and extracellular metabolite profiles of *Acinetobacter calcoaceticus* DT1 and associated functional pathways. (**a**) Hierarchical clustering heatmap of metabolites identified by LC–HRMS QTOF in

the intracellular (pellet) and extracellular (supernatant) fractions of DT1, represented as log_2-transformed peak area values. (**b**) KEGG pathway enrichment analysis of the differentially produced metabolites from (**a**), highlighting biological processes associated with plant growth promotion and stress resilience.

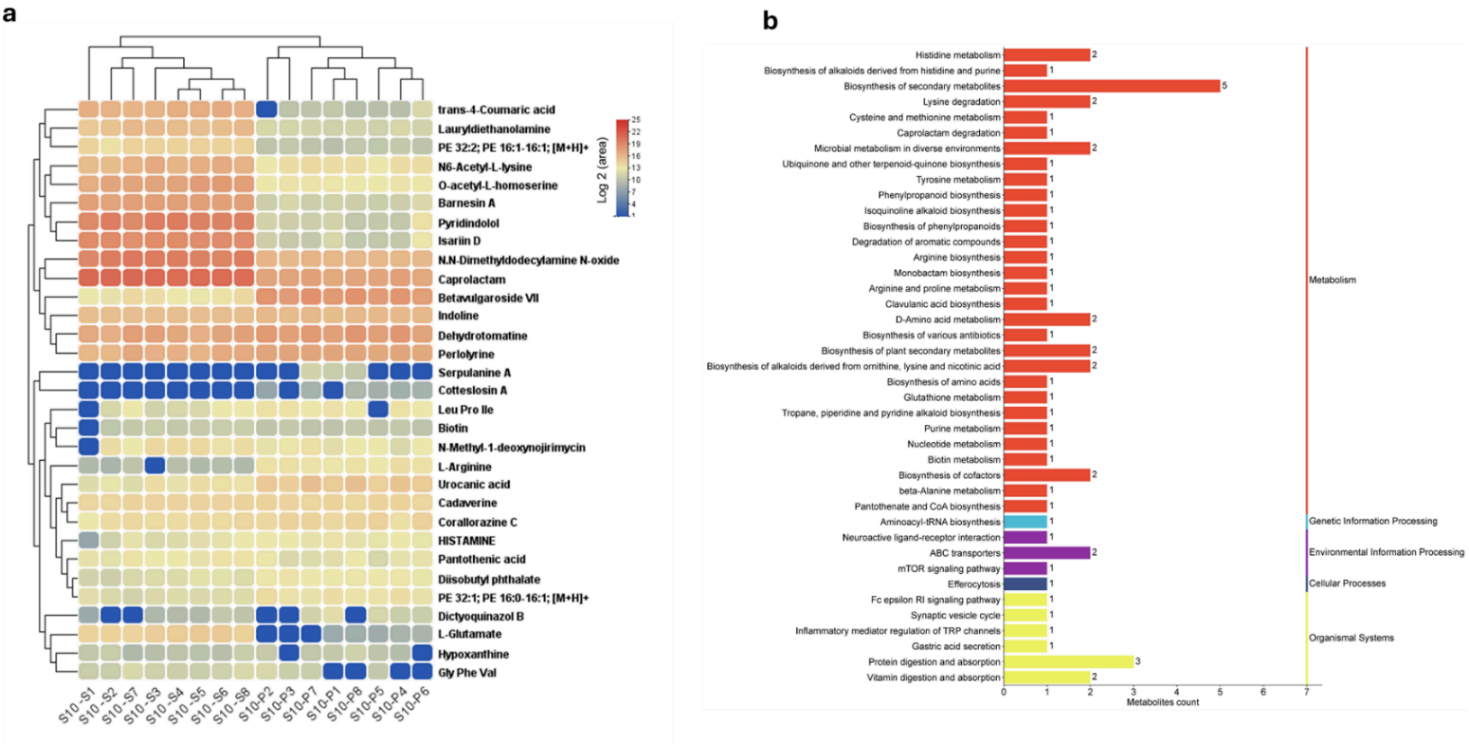

Figure 11

Intracellular and extracellular metabolite profiles of *Citrobacter braakii* S10 and associated functional pathways. (**a**) Hierarchical clustering heatmap of metabolites identified by LC–HRMS QTOF in the intracellular (pellet) and extracellular (supernatant) fractions of S10, presented as log_2-transformed peak area values. (**b**) KEGG pathway enrichment analysis of the differentially abundant metabolites from (**a**), showing functional associations with plant growth-promoting and stress-responsive pathways.

Supplementary Files

This is a list of supplementary files associated with this preprint. Click to download.

- SupTableANIandDDH.xlsx
- SuptablemetabolitesPGP.xlsx
- SuptablePGPtraitsce.xlsx